

March 2023

Remote Medical Diagnosis via Infrared Thermography and Augmented Reality

Frederick M. Selkey
University of South Florida

Follow this and additional works at: <https://digitalcommons.usf.edu/etd>



Part of the [Biomedical Engineering and Bioengineering Commons](#), [Computer Sciences Commons](#), and the [Electrical and Computer Engineering Commons](#)

Scholar Commons Citation

Selkey, Frederick M., "Remote Medical Diagnosis via Infrared Thermography and Augmented Reality" (2023). *USF Tampa Graduate Theses and Dissertations*.
<https://digitalcommons.usf.edu/etd/10449>

This Thesis is brought to you for free and open access by the USF Graduate Theses and Dissertations at Digital Commons @ University of South Florida. It has been accepted for inclusion in USF Tampa Graduate Theses and Dissertations by an authorized administrator of Digital Commons @ University of South Florida. For more information, please contact digitalcommons@usf.edu.

Remote Medical Diagnosis via Infrared Thermography and Augmented Reality

by

Frederick M. Selkey

A thesis submitted in partial fulfillment
of the requirements for the degree of
Master of Science
Department of Electrical Engineering
College of Engineering
University of South Florida

Major Professor: Stephen Saddow, Ph.D.
Mark Jaroszeski, Ph.D.
Sriram Chellappan, Ph.D.

Date of Approval:
March 13, 2023

Keywords: Contagious, Upper Respiratory Tract Infection,
Mobile, Kiosk, Scanner

Copyright © 2023, Frederick M. Selkey

Dedication

This thesis is dedicated to those who were affected by the global pandemic known as Covid-19.

Acknowledgments

This thesis project was entirely self-funded. There are no acknowledgments given for funding. No conflicts of interest to be declared.

Table of Contents

| | |
|------------------------------------------|------|
| List of Tables | iv |
| List of Figures | v |
| List of Abbreviations | viii |
| Abstract | x |
| Chapter 1: Introduction | 1 |
| 1.1 Fever Screening | 1 |
| 1.2 Problem Statement | 2 |
| 1.3 Organization | 3 |
| Chapter 2: Background | 5 |
| 2.1 Conduction | 6 |
| 2.2 Convection | 7 |
| 2.3 Radiation | 8 |
| 2.4 Black Bodies | 10 |
| 2.5 Emissivity | 11 |
| 2.6 Thermoregulation | 13 |
| 2.7 URTIs | 15 |
| 2.8 Lacrimal Apparatus | 16 |
| 2.9 Summary | 18 |
| Chapter 3: Hardware | 19 |
| 3.1 History of Thermal Imagers | 20 |
| 3.2 FLIR ONE Pro | 21 |
| 3.3 TOPDON TCView TC001 | 24 |
| 3.4 Raspberry Pi | 25 |
| 3.5 Summary | 27 |
| Chapter 4: Medical IRT | 28 |
| 4.1 History of Thermography | 29 |
| 4.2 Burn Wounds | 31 |
| 4.3 Broken Bones | 32 |
| 4.4 Complex Regional Pain Syndrome | 33 |
| 4.5 Focal Infections | 34 |
| 4.6 Summary | 35 |

| | |
|-------------------------------------------------------------|----|
| Chapter 5: Related Work | 36 |
| 5.1 Acute Respiratory Illness | 37 |
| 5.2 Covid-19 | 38 |
| 5.3 ER Triage | 39 |
| 5.4 Remote Heart Rate | 40 |
| 5.5 Remote Respiration Rate | 42 |
| 5.6 Remote Vital Signs | 44 |
| 5.7 Summary | 45 |
| Chapter 6: Application Software | 46 |
| 6.1 Nginx..... | 47 |
| 6.2 TLS Certificates | 48 |
| 6.3 RTMP..... | 50 |
| 6.4 Python | 51 |
| 6.5 OpenCV | 52 |
| 6.6 Flask..... | 53 |
| 6.7 JavaScript..... | 54 |
| 6.8 Video Streaming | 56 |
| 6.9 Summary | 58 |
| Chapter 7: Computer Vision | 59 |
| 7.1 History of Facial Recognition..... | 60 |
| 7.2 RGB Facial Landmarks..... | 62 |
| 7.3 Homography Matrix..... | 63 |
| 7.4 IRT Facial Landmarks | 65 |
| 7.5 Color Space..... | 67 |
| 7.6 Euclidean Distance..... | 68 |
| 7.7 Grayscale..... | 69 |
| 7.8 Results..... | 71 |
| 7.9 Summary | 73 |
| Chapter 8: Conclusions | 74 |
| 8.1 Discussion | 75 |
| 8.2 Limitations | 76 |
| 8.3 Applications | 77 |
| 8.4 Further Development | 78 |
| 8.5 Final Thoughts | 79 |
| References..... | 80 |
| Appendix A: Block Diagram of Processing a Video Stream..... | 84 |
| Appendix B: Doll Head Simulation..... | 85 |
| Appendix C: Nasolacrimal Vector..... | 87 |

| | |
|-----------------------------------------------|----|
| Appendix D: Kiosk and Mobile Diagrams | 91 |
| Appendix E: Kiosk and Mobile Prototypes | 92 |

List of Tables

| | | |
|------------|------------------------------------------------------------|---|
| Table 2.1: | Effective thermal diffusivity measured in pig tissue | 6 |
| Table 2.2: | Types of infrared radiation organized by wavelength | 9 |

List of Figures

| | | |
|-------------|--------------------------------------------------------------------------------|----|
| Figure 2.1: | Diagram of temperature gradient illustrating the flow of heat | 6 |
| Figure 2.2: | Diagram of human hand illustrating the convection of heat in air | 7 |
| Figure 2.3: | Diagram of electromagnetic (EM) radiation..... | 8 |
| Figure 2.4: | Emissive power of a black body radiator at various temperatures | 10 |
| Figure 2.5: | Diagram of a Leslie cube demonstrates the effect of emissivity | 11 |
| Figure 2.6: | Block diagram of a biological temperature control mechanism | 13 |
| Figure 2.7: | Graph of symptoms with respect to days since exposure | 15 |
| Figure 2.8: | Diagram of the lacrimal apparatus | 16 |
| Figure 3.1: | Conceptual diagram of a bolometer | 20 |
| Figure 3.2: | Picture of FLIR ONE Pro thermal camera..... | 21 |
| Figure 3.3: | Picture of TOPDON TCView TC001 thermal camera..... | 24 |
| Figure 3.4: | Picture of Raspberry Pi 4 Model B | 25 |
| Figure 4.1: | IRT diagram of female breast demonstrating a cancerous lesion | 29 |
| Figure 4.2: | Multispectral diagram illustrating the analysis of burn wounds..... | 31 |
| Figure 4.3: | IRT diagram of distal forearm fracture healing | 32 |
| Figure 4.4: | IRT diagram illustrating the healing process of CRPS..... | 33 |
| Figure 4.5: | Diagram illustrating the use of IRT to find hidden focal infections | 34 |
| Figure 5.1: | IRT diagram of face illustrating fever and normal conditions..... | 37 |
| Figure 5.2: | IRT diagram of healthy patient (A) compared to patient with Covid-19 (B) | 38 |
| Figure 5.3: | Core vs peripheral body temperature measurements | 39 |

| | | |
|--------------|----------------------------------------------------------------------|----|
| Figure 5.4: | Superficial arteries of the face and neck | 40 |
| Figure 5.5: | IRT diagram of remote RR with a BSI | 42 |
| Figure 5.6: | Diagram of RGB and IR cameras measuring vital signs | 44 |
| Figure 6.1: | Block diagram illustrating the use of nginx as a reverse proxy | 47 |
| Figure 6.2: | Block diagram illustrating the use of TLS Certificates | 48 |
| Figure 6.3: | Block diagram of an RTMP server | 50 |
| Figure 6.4: | Block diagram illustrating the use of Python..... | 51 |
| Figure 6.5: | Block diagram illustrating the use of OpenCV..... | 52 |
| Figure 6.6: | Block diagram illustrating the use of Flask | 53 |
| Figure 6.7: | Block diagram illustrating the use of JavaScript | 54 |
| Figure 6.8: | Illustration of unicast streaming..... | 56 |
| Figure 7.1: | Block diagram of facial recognition | 60 |
| Figure 7.2: | Example of facial landmark annotation on a standard model..... | 62 |
| Figure 7.3: | Diagram of two cameras recording a human face | 63 |
| Figure 7.4: | Example of facial landmark annotation on a thermal model | 65 |
| Figure 7.5: | Illustration of additive and subtractive color spaces..... | 67 |
| Figure 7.6: | Diagram of the Euclidean distance in two dimensions..... | 68 |
| Figure 7.7: | Illustration of RGB image decomposition into grayscale..... | 69 |
| Figure 7.8: | Thermal image of a healthy face..... | 71 |
| Figure 7.9: | Thermal image of a URTI infected face | 71 |
| Figure 7.10: | RGB image of oral cavity | 72 |
| Figure 7.11: | Image of antigen test for Covid-19 | 72 |
| Figure A.1: | Block diagram illustrates the processing of a video stream..... | 84 |

| | | |
|-------------|----------------------------------------------------------------------------|----|
| Figure B.1: | Doll head simulation with negative AR diagnosis..... | 85 |
| Figure B.2: | IR doll head simulation showing negative ROIs | 85 |
| Figure B.3: | Doll head simulation with positive AR diagnosis..... | 86 |
| Figure B.4: | IR doll head simulation showing positive ROIs | 86 |
| Figure C.1: | Side profile of human face | 87 |
| Figure C.2: | The nasolacrimal vector drawn on side profile of human face..... | 87 |
| Figure C.3: | The nasolacrimal vector drawn on an RGB diagram..... | 88 |
| Figure C.4: | The nasolacrimal vector drawn on an IRT diagram..... | 88 |
| Figure C.5: | TOPDON TCView TC001 thermal image with facial landmarks..... | 89 |
| Figure C.6: | TOPDON TCView TC001 thermal image with nasolacrimal vector..... | 89 |
| Figure C.7: | Positive FLIR ONE Pro thermal image with nasolacrimal vector..... | 90 |
| Figure C.8: | Positive FLIR ONE Pro thermal image with nasolacrimal ROI..... | 90 |
| Figure D.1: | Diagram illustrating the mobile app for augmented reality diagnosis | 91 |
| Figure D.2: | Diagram illustrating the kiosk device for augmented reality diagnosis..... | 91 |
| Figure E.1: | Android mobile phone prototype demonstration | 92 |
| Figure E.2: | Kiosk prototype demonstration..... | 92 |

List of Abbreviations

| Abbreviations | Definitions |
|----------------------|-------------------------------------------------------------|
| ADA | Americans with Disabilities Act of 1990 |
| AIDS | Acquired Immunodeficiency Syndrome |
| AR | Augmented Reality |
| BSI | Breathing Sorption Indicator |
| BVP | Blood Volume Pulse |
| CMYK | Cyan Magenta Yellow Black |
| CPU | Central Processing Unit |
| CRPS | Complex Regional Pain Syndrome |
| CV | Computer Vision |
| EM | Electromagnetic |
| ER | Emergency Room |
| FFT | Fast Fourier Transform |
| FIR | Far Infrared |
| FLIR | Forward Looking Infrared |
| GPU | Graphics Processing Unit |
| HIPAA | Health Insurance Portability and Accountability Act of 1996 |
| HIV | Human Immunodeficiency Virus |
| HR | Heart Rate |
| HTML | Hypertext Markup Language |
| HTTP | Hypertext Transfer Protocol |
| HTTPS | Hypertext Transfer Protocol Secure |
| InSb | Indium antimonite |
| IR | Infrared |
| IRT | Infrared Thermography |
| ISO | International Organization for Standardization |
| JSON | JavaScript Object Notation |
| JWT | JSON Web Token |
| LBP | Local Binary Pattern |
| LWIR | Long-wave Infrared |
| MB | Megabyte |
| MITM | Man-in-the-Middle |
| MSX® | Multi-Spectral Dynamic Imaging |
| MWIR | Mid-Wave Infrared |
| NIR | Near Infrared |
| OpenCV | Open-Source Computer Vision |
| OS | Operating System |
| OST | Ocular Surface Temperature |
| OTC | Over the Counter |

| | |
|-------|-----------------------------------------|
| PCA | Principal Component Analysis |
| PIP | Preferred Installer Program |
| RTMP | Real-Time Messaging Protocol |
| RGB | Red Green Blue |
| ROI | Region of Interest |
| RR | Respiration Rate |
| SARS | Severe Acute Respiratory Syndrome |
| SWIR | Short-Wave Infrared |
| SBC | Single Board Computer |
| SEIRT | Sorption Enhanced Infrared Thermography |
| TLS | Transport Layer Security |
| UI | User Interface |
| URTI | Upper Respiratory Tract Infection |
| USB | Universal Serial Bus |

Abstract

Fast, accurate, and non-invasive diagnostic techniques are required by the medical industry to increase the success of medical treatments and enhance the quality of patient care. Medical IRT has been demonstrated reasonably effective at diagnosing and monitoring several physiological conditions. Diversities in the human body, physical and psychological condition, measurement equipment, and environment all influence the sensitive readings obtained by passive IR measurement devices. New standards for medical IRT and fever screening have been demonstrated effective, but there is limited adherence to the guidelines [36]. Absolute temperature readings require regular calibration checks and can easily be thrown off by noise. Finally, limited IRT images and data are available for training ML and DL models, and annotating the images manually is time consuming. New methods are required to annotate medical IRT images and evaluate them for diagnostic potential. Multiple vital signs are required for making more accurate assessments of Upper Respiratory Tract Infections. An AR app is created to provide remote measurement of vital signs and detect contagious diseases in real-time.

Chapter 1: Introduction

EM radiation is an increasingly important part of the medical industry. Doctors use ambient light to examine patients for visible signs of injury or disease, before subjecting them to a battery of tests. These include mechanical, chemical, and electromagnetic methods. The presence of a rash is frequently used as an initial diagnostic tool. This is due to the quick and inexpensive nature of visual testing, and the distinctive appearance of most rashes. But human vision is limited to the visible spectrum of light. Augmenting the visible spectrum with infrared sensors can serve to enhance the diagnostic capabilities of experienced doctors. Infrared thermography reveals temperature patterns in the human body that can appear symmetrical or asymmetrical. These are akin to a rash that appears outside the visible spectrum of light.

1.1 Fever Screening

Ring et al discuss the standards and implications of thermal imaging for fever screening [36]. Originally, core body temperature was measured with a thermometer [36]. Infrared radiometers are now commonly used to infer core body temperature by measuring inner ear temperature [36]. In 2006, airports began screening for fevers with infrared cameras, but do not necessarily use valid techniques [36]. The International Organization for Standardization (ISO) published two standards in 2008-2009 to deal with infrared fever screening [36]. The new standards indicate that core body temperature should be read by measuring the average temperature of at least 9 pixels centered around the inner canthus of the eye [36]. Ring et al used clinical studies to demonstrate that the methods outlined by the new ISO standards are effective for fever screening [36].

1.2 Problem Statement

Infrared Thermography (IRT) is a promising technology for non-invasive medical diagnosis and monitoring of physiological conditions. It has a long history of providing remote temperature measurements and inferring medical diagnosis. Poor resolution cameras, inaccuracies of calibration, and the absence of standardization all contribute to a lack of adoption by the medical community. New standards have been proposed but are not necessarily being enforced or followed. Patients need to be allowed enough time to establish thermal equilibrium with tightly controlled environmental conditions inside the test facility. Calibration checks are required to ensure accurate temperature measurements, which pose ongoing maintenance costs. The true cost of IRT diagnosis is incurred from false readings. A false positive medical diagnosis can send a patient for radiological evaluation when it would otherwise not be recommended. A false negative medical diagnosis can instill a false sense of security, delaying or stopping a patient from receiving a more accurate diagnosis so that they may begin treatment. False reading of IRT fever screening in the airport can unnecessarily delay travel plans and incur legal liability.

Human interpretation of medical thermography images requires professional knowledge and experience. Using advanced ML and DL algorithms, computer imaging software can now perform medical diagnosis automatically. They are commonly used with standard RGB images, where large datasets of high-resolution images are freely available. The low pixel resolution, contour details, and limited datasets makes it more difficult to train ML and DL algorithms on IRT images. The computational requirements to run these algorithms limit the portability of IRT systems. Without adequate methods to handle calibration differences between various IR cameras, and provide the computational requirements for computer vision libraries, the benefits of IRT may not be fully realized.

1.3 Organization

We start Chapter 2 with a background of thermal energy and electromagnetic (EM) radiation. The emission of thermal energy from a surface and its relationship with temperature is discussed. Thermoregulation introduces the biological production of thermal radiation and establishes the narrow range of temperature in healthy subjects [3]. Finally, we discuss the Lacrimal Apparatus and the human immune system response to respiratory infection [9]. Chapter 3 continues with the hardware utilized in this project. It begins with a brief history of thermal imagers [38]. Then we discuss the FLIR ONE Pro thermal camera, with some of its applications [14] [15]. The FLIR ONE Pro is compared to another consumer-friendly thermal camera, the SEEK Compact Pro [24]. Afterwards, we explain why the TCView TC001 thermal camera was ultimately chosen for this thesis project. Finally, we discuss the Raspberry Pi as a low-cost solution for maintaining portability in our IRT system [1] [20] [41].

Chapter 4 begins with a brief history behind medical IRT. Research from those early days mainly focused on diagnosing breast cancer [16] [26] [39]. Then, we discuss the use of IRT to evaluate burn wounds [21]. It is interesting how IRT can be used to monitor the treatment of conditions ranging from broken bones [5] to Complex Regional Pain Syndrome [7]. Finally, we learn how IRT can be used to find hidden focal infections that elude conventional diagnostic techniques [18]. Chapter 5 evaluates the most similar works regarding Infrared Thermography (IRT) and remote medical diagnosis. It begins with work aimed at using IRT to measure core body temperature using the lacrimal caruncles to diagnose respiratory illness [29] [45]. This sets up the premise that forehead temperature alone is not enough for diagnosis of contagious respiratory infections. We proceed with the use of IRT for ER triage [2]. This demonstrates the importance of peripheral temperature and provides another diagnostic possibility. IRT videos are

used to remotely measure vital signs like Heart Rate (HR) [17] [33] and Respiration Rate (RR) [10] [44]. Finally, the diagnosis is improved by combining the measurements of remote vital signs with that of core body temperature [31].

Chapter 6 implements the software required to build the application and securely host everything online. It begins with a brief discussion of using nginx as a reverse proxy server. Then, we use Let's Encrypt to secure connections to the web server. The nginx server requires modification to handle video streaming formats such as Real Time Messaging Protocol (RTMP). Next, we apply Python, and the libraries necessary for image processing. This includes a discussion regarding OpenCV and Flask. We use JavaScript to provide user interface (UI) and authentication. JSON Web Tokens (JWTs) are used to protect static resources on the server. Finally, we discuss MJPEG streaming and the resulting bandwidth problem. Chapter 7 proceeds with the algorithms required for image processing. It begins with a brief history of facial recognition. Then, we discuss machine learning libraries to annotate facial landmarks. Homography matrixes are considered to translate the facial landmark locations onto thermal images. We proceed to discuss color spaces and the use of grayscale to calculate temperature differentials. Then, we discuss facial landmark detection on thermal images. Finally, we conclude with a discussion of results.

Chapter 8 concludes this thesis paper. The development process is illustrated to show stepwise improvements to the algorithm. Then, we mention the limiting factors of the device's operation. Further testing is warranted to verify the limiting factors and improve the algorithm. We proceed with some of the possible applications of the proposed device. The development process is outlined regarding future work. The paper concludes with final thoughts regarding medical IRT and the new application.

Chapter 2: Background

A background of physics facilitates an understanding of thermal energy. Heat is known to transfer via three distinct mechanisms. Conduction is the transfer of heat that takes place between two objects that are touching [37]. Convection is the transfer of heat through the molecular motion of fluid between two objects [37]. Radiation is the transfer of heat through the emission of electromagnetic waves [37]. Both convection and radiation allow for remote temperature measurements [37]. The latter is preferred due to the skin's high emissivity and the non-invasive nature of passive sensors.

Black body radiators most accurately describe the radiating properties of human skin. The wavelength of radiation emitted with maximum power can be calculated by temperature. Emissivity, the ability of a surface to radiate thermal energy, is the single most important property of thermal imaging. The tear film across the ocular surface decreases the emissivity of the eyes. Core body temperatures should be recorded by measuring the lacrimal caruncles, not the ocular surface.

A background of biological processes helps facilitate an understanding of the relationship between thermal energy and disease. Thermoregulation is the important property of mammals and other endotherms that maintain core body temperatures within a narrow range of operation. Fever and inflammation are the human body's natural reaction to infection. Inflammatory cytokines are biomolecules which cause inflammation and fever. They are responsible for elevating core body temperature during Upper Respiratory Tract Infections (URTIs). The Lacrimal Apparatus is examined for potential diagnostic properties.

2.1 Conduction

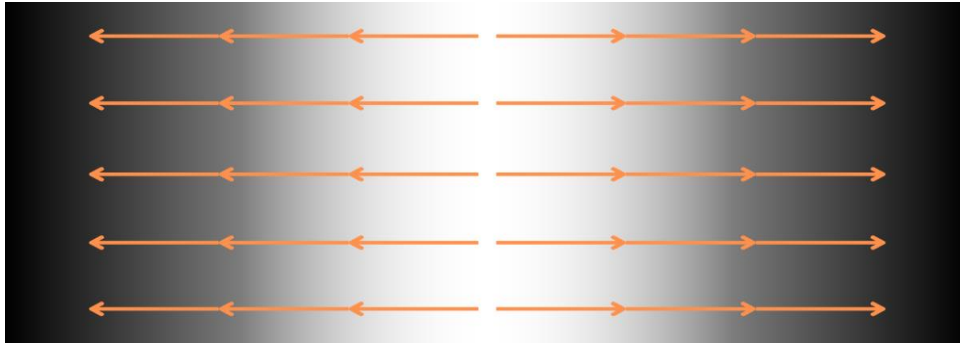


Figure 2.1: Diagram of temperature gradient illustrating the flow of heat. Thermal energy conducts from regions of high to low value. In this case, from the middle out.

Thermal conduction refers to the flow of heat energy through a material. It is responsible for thermal energy transferred between objects that are touching. This is the mechanism of heat transfer that thermistors use to measure temperature. First, contact is made with the object of interest. Then, time is allowed to pass for heat to flow via conduction and establish thermal equilibrium. Molecular vibrations due to thermal energy spread through a material as a wave. These waves of molecular vibration can be thought of similarly to electromagnetic waves. Waves of thermal energy within a material are discretized into packets of energy, or quanta, called phonons [30]. The conduction of heat follows a gradient from regions of high to low temperature. Thermal diffusion refers to the flow of temperature through a material and is related to thermal conductivity by specific heat [34]. Temperature will flow through the material at a rate established by its thermal diffusivity.

Table 2.1: Effective thermal diffusivity measured in pig tissue. Modified from [34].

| Tissue | Skin | Fat | Liver |
|----------------------------------------|------|------|-------|
| Diffusivity (mm^2/s) | 0.41 | 0.35 | 0.54 |

2.2 Convection

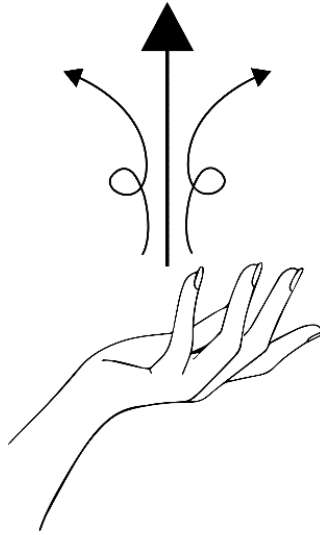


Figure 2.2: Diagram of human hand illustrating the convection of heat in air.

Convection refers to the transfer of heat through the motion of molecules between two objects. It occurs spontaneously due to the dependence of buoyancy on temperature. Higher temperatures cause the molecules of a fluid to vibrate with more energy. The energetic particles are more likely to collide with each other, causing separation and a loss of density. This is referred to as free or natural convection. Heat loss can also occur through forced convection. Fans or pumps actively moving fluid between two objects can cause the exchange of heat to occur more rapidly. Environmental factors such as the wind or ocean currents can also cause force convection. The convection of heat is a normal method of heat loss from a hot body, and part of the human thermoregulatory system. The effects of convection should be minimized to allow thermal equilibrium and prevent inaccurate temperature measurements. Infrared thermography should be used cautiously in circumstances of forced convection such as in the presence of mechanical fans or high winds. It is important for a body to reach thermal equilibrium before measuring its temperature.

2.3 Radiation

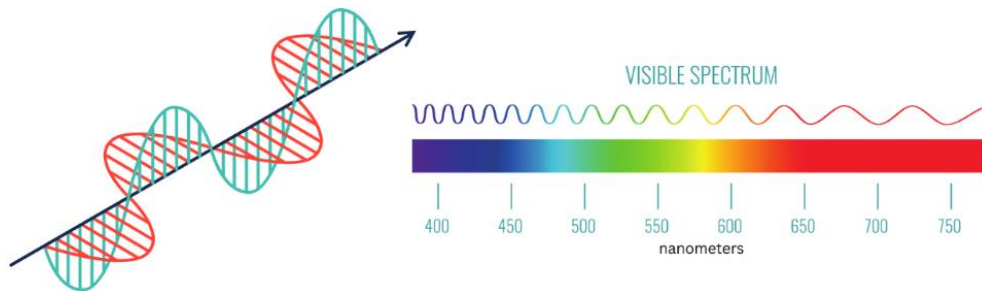


Figure 2.3: Diagram of electromagnetic (EM) radiation. Illustrating the perpendicular vector components of light next to the visible wavelengths of light.

Electromagnetic radiation is the propagation of light through space. It can be broken down into perpendicular vectors of electric and magnetic components. These vectors oscillate in a synchronized manner depending on the frequency. The direction of propagation is determined by the right-hand rule. EM radiation can mimic the behavior of either a wave or a particle. To consider the particulate nature of light, it can be thought of as discrete energy packets, or quanta, called photons. The quantization of waves results from applying boundary conditions to a particular solution of Schrodinger's equation [30]. This explains the wave-particle duality of light.

Light is used in medicine for a variety of diagnostic and treatment purposes. Non-ionizing radiation, containing the visible, microwave, and radio wave spectrums are generally considered safe. There is not enough energy to ionize molecules or break molecular bonds. Visible Red Green Blue (RGB) light is used by experienced doctors to visually examine patients. Magnetic Resonance Imagers (MRIs) employ large magnetic fields and radio waves to diagnose the soft tissues in the human body. Low frequency radio waves can also be used as a treatment to stimulate the regrowth of broken bones. Mitochondria may be sensitive to EM fields due to iron

rich proteins inside the membrane [19]. EM fields promote the growth and function of osteogenic cells by inducing mitochondrial respiratory complex I which stimulates the mitochondrial OxPhos activity [19]. Ionizing radiation has enough energy to ionize molecules and break the bonds between strands of DNA. Ionizing radiation contains the UV, X-ray, and gamma ray spectrums of light. Flashed X-rays are used to diagnose internal skeletal structures. Continuous beams of X-rays are used as a treatment to kill cancerous tumor growths.

Thermal radiation refers to the band of EM spectrum with a wavelength between 0.1 to 100 μm [3]. This includes IR, visible, and parts of the UV spectrum [3]. Most of the radiation emitted by the human body is typically in the range of 2 to 20 μm , and peaks in the range of 9 to 10 μm [3]. This can be confirmed by Plank’s law of black body radiators, which would use a temperature of approximately 300 K [3]. Emission of thermal radiation from a surface is subsequently discussed.

Table 2.2: Types of infrared radiation organized by wavelength. Modified from [4].

| Name | Abbreviation | Wavelength (μm) | Frequency (THz) | Energy (meV) | Temperature (K) |
|---------------------|--------------|------------------------------|-----------------|--------------|-----------------|
| Near Infrared | NIR | 0.75 – 1.4 | 214 – 400 | 886 – 1653 | 3864 – 2070 |
| Short-Wave Infrared | SWIR | 1.4 – 3 | 100 – 214 | 413 – 886 | 2070 – 966 |
| Mid-Wave Infrared | MWIR | 3 – 8 | 37 – 100 | 155 – 413 | 966 – 362 |
| Long-Wave Infrared | LWIR | 8 – 15 | 20 – 37 | 83 – 155 | 362 – 193 |
| Far Infrared | FIR | 15 – 1000 | 0.3 – 20 | 1.2 – 83 | 193 – 3 |

2.4 Black Bodies

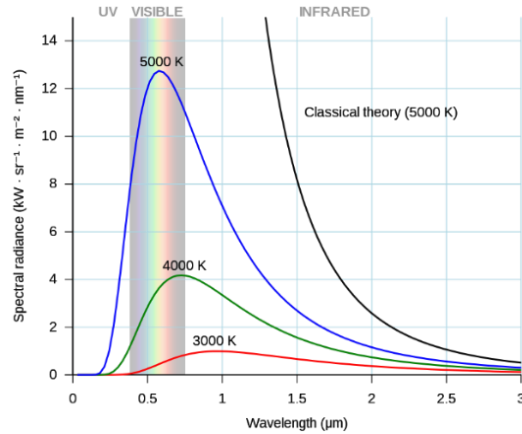


Figure 2.4: Emissive power of a black body radiator at various temperatures. This graph depicts the family of curves given by Planck's Law. Reprinted from [11]. Public Domain.

A black body radiator is the ideal version of a physical material with high emission and absorption properties of EM radiation. Planck's Law describes the behavior of a black body radiator with respect to frequency ν and temperature T [22]. Where h represents Planck's constant, k represents Boltzmann's constant, and c represents the speed of light [22].

$$E(\nu, T) = \frac{h\nu^3}{c^2} \cdot \frac{1}{\exp\left(\frac{h\nu}{kT}\right) - 1}$$

which yields the emissive power at a given wavelength and temperature [22]. Total emissive power from a black body radiator at a given temperature is found by integrating Planck's law across all frequencies. This is known as the Stefan Boltzmann law. Here, σ represents the Stefan Boltzmann constant.

$$E = \sigma T^4$$

2.5 Emissivity

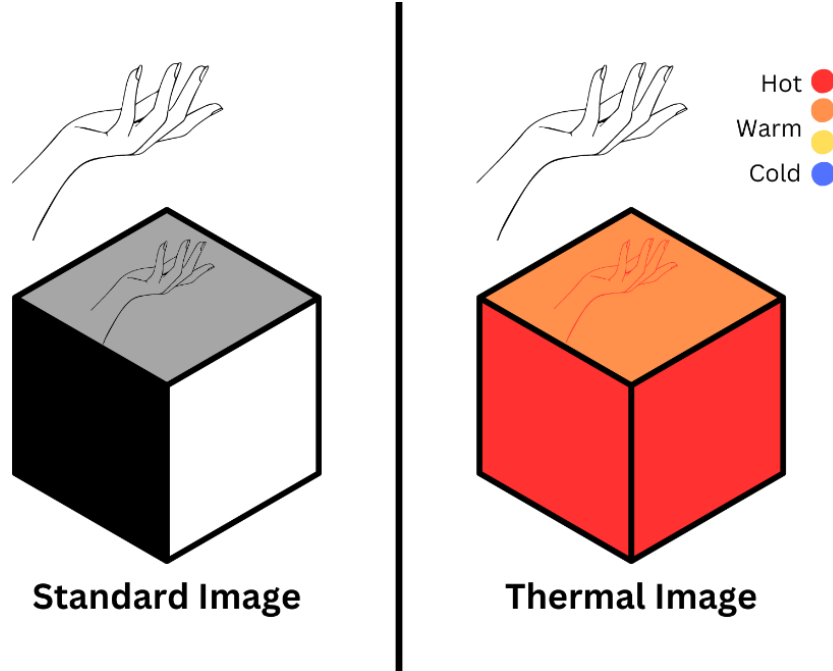


Figure 2.5: Diagram of a Leslie cube demonstrates the effect of emissivity. Note that the colors black and white demonstrate similar values of temperature on a thermal image. Heat can be reflected on polished surfaces.

Different materials, surface textures, and colors all radiate thermal energy with different levels of efficiency. To remotely infer a temperature with infrared radiation, we need consider how well the surface can emit heat energy. This is called emissivity, the measure of a surface's ability to radiate energy as heat. An ideal black body radiator has an emissivity equal to 1 but real materials have real emissivity values below 1 [28]. Therefore, emissivity for real materials is always between 0 and 1. The Stefan Boltzmann law can be modified for real materials by providing a constant ϵ , for emissivity [28]. Note that the power radiating from a black body is still exponential with temperature.

$$E = \epsilon\sigma T^4$$

The Leslie cube is a tool to simultaneously examine the emissivity of different materials. Since emissivity depends on the surface's color and material properties, it can demonstrate the difficulty in measuring temperature with IR. The Leslie cube shows that white and black colors have similar values of emissivity. This is why heat sinks are frequently powder coated either black or white. It also demonstrates reflection as an artifact of noise. Note the reflected image of a hand in the thermal image above, resulting from a polished surface. The reflection of thermal radiation is similar to the visual spectrum. It is important to reduce sources of noise and interference for accurate measurements. Faces can vary widely in size, shape, and color. These biological differences do not impact absolute temperature measurements taken remotely. But variations in the environment and thermoregulation can influence remote temperature measurements. For these reasons, we consider relative temperature differences over absolute values when measuring temperatures remotely.

Tan et al discuss the physics behind IR thermography for the purpose of measuring Ocular Surface Temperature (OST). They point out that water acts like a black body radiator, depending on the thickness of the film [42]. However, at thicknesses closer to that of human tear film, IR transmission in the range of human body heat emission is nearly zero [42]. The tear film is the layer of water that hydrates the surface of the eyes. It is produced by the lacrimal glands and drained by the nasolacrimal ducts. The lacrimal apparatus is discussed at the end of chapter 2. Thermal energy radiated by the cornea is likely to be absorbed by the tear film [42]. This is due to the poor emissivity of water in thin sheets. These results indicate why core body temperature cannot be taken by remote IR measurements of the center cornea. The lacrimal caruncles and eyelids provide a more accurate IR measurement of core temperature. This is due to the absence of tear film, and high emissivity of the skin.

2.6 Thermoregulation

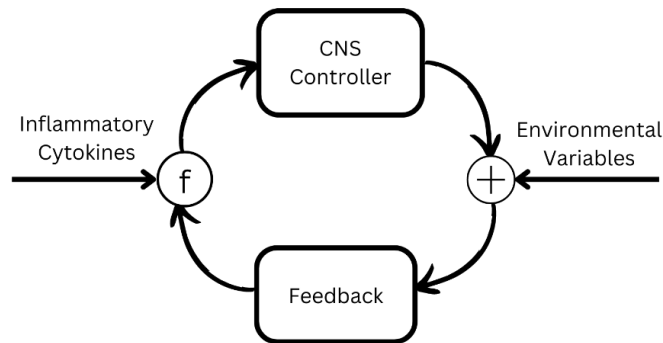


Figure 2.6: Block diagram of a biological temperature control mechanism. A simplified example to illustrate how temperature is maintained by the human body, resulting in thermoregulation.

Endotherms are animals that can control their own body temperature. Thermoregulation is the biological process which controls the temperature in endotherms. Regulated by the hypothalamus, it is vital to the maintenance of homeostasis. Disruption in thermoregulation has been known for thousands of years to be an indicator of disease. Fevers are a result of the body attempting to fight infection. Shivering is a well-known symptom of being cold or feverish. This is the result of thermoregulatory systems attempting to raise core body temperature. As temperatures increase, so does the speed of metabolic processes. If temperatures go too high, essential proteins begin to unravel. The three mechanisms of heat transfer are used by endotherms to prevent the excessive buildup of heat. Conduction mainly occurs through exposed feet unless in a sitting or prone position. Convection and radiation are primarily controlled by hair and clothing. Humans are capable of sweating, and therefore also lose heat to the environment through evaporation. Metabolic processes through anabolism and catabolism result in the stability of core body temperature. The oxidation of ATP molecules is an exogenic reaction and a source of metabolic heat.

Studying the effects of thermoregulation provides insight into how the body responds to stress. Bouzida et al use IRT to study the thermoregulatory processes of the human body [3]. They utilized a FLIR Phoenix type MWIR camera, operating in the 3-5 μm spectrum, with a resolution of 640 x 512 pixels [3]. Even though MWIR cameras do not operate in the peak range of emissions produced by the human body, they can still provide value to applications of medical IRT. The venous system allows blood to carry oxygen and nutrients throughout the body and therefore provides an important mechanism of heat flow. It is an important system to consider when studying thermoregulation in mammals. Bouzida et al, measured the temperature of vein pixels (VPs) for a brief time following the planned disruption of the body's thermoregulatory system by one of two different methods.

Plethysmography and cold stress techniques were independently evaluated to observe the effects of human thermoregulation [3]. Plethysmography is a non-invasive technique used to detect venous thrombosis [3]. It examines blood flow by applying periodic mechanical pressure to a tourniquet-like device designed to block the flow of blood through the venous system. Cold stress was also used to evaluate the thermoregulatory processes after a localized part of the peripheral system was cooled [3]. Both venous occlusion and cold temperature cause vasoconstriction, which appears as dark (cooler) regions on a grayscale thermal image [3]. Vasoconstriction is a physiological response characterized by a temporary narrowing of the veins. It restricts blood flow to conserve heat throughout the body. Both methods obtained similar results, illustrating a cooling action in the stressed hand, and a warming action in the non-stressed hand. Applications of cold and pressure provide similar physiological responses to stress. This is the result of thermoregulatory processes working to balance the temperature of the human body.

2.7 URTIs

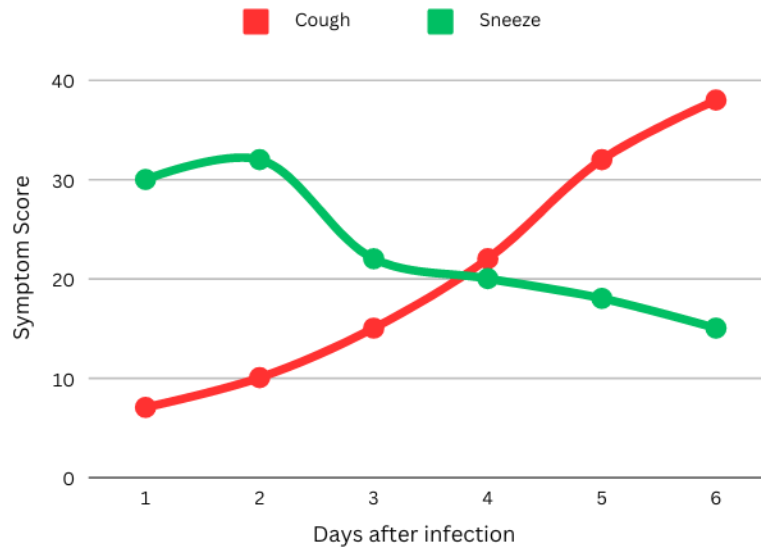


Figure 2.7: Graph of symptoms with respect to days since exposure. Demonstrates that sneezing is predominant in the early days of URTIs. Modified from [9].

Eccles reviewed the mechanisms that cause cold and flu symptoms in humans [9]. Upper Respiratory Tract Infections (URTI) are some of the most frequently encountered contagious diseases [9]. They are highly contagious due to the coughing, sneezing, and wiping of contaminated mucus. There are over 200 different types of viruses which are known to cause URTIs in humans [9]. Covid-19 and other pandemics represent various types of URTIs. In experiments, adults rarely contract a fever in the beginning stages of a URTI [9]. This provides our first evidence that fever alone is not a good early indicator of contagious infections like URTIs. According to Figure 2.7, the symptom of sneezing is a better early warning sign of URTI in adults. Coughing does not take precedence until the later stages of infection. But just because someone sneezes, does not mean they are contagious with a URTI. Allergies create a case where sneezing as a symptom does not coincide with contagious URTIs. This reinforces the need for multiple symptoms to be considered before making a diagnosis.

2.8 Lacrimal Apparatus

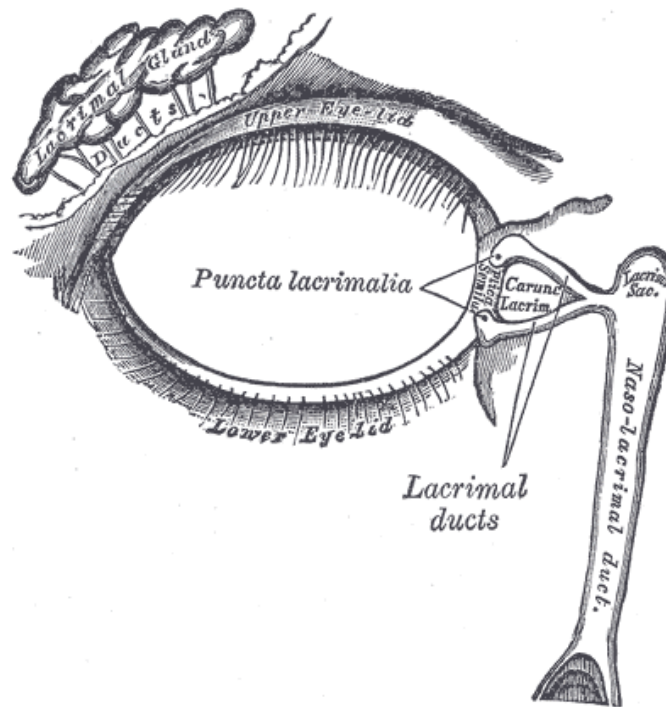


Figure 2.8: Diagram of the lacrimal apparatus. The lacrimal glands produce tears, and the lacrimal ducts provide drainage around the ocular surface. Reprinted from [13]. Public Domain.

The lacrimal apparatus is an anatomical system of the human body responsible for the drainage and production of ocular tears. It consists of the nasolacrimal ducts, the lacrimal caruncles, and the lacrimal glands. Properly functioning, the system prevents dry eyes and acts as a first line of defense against pathogens. Dysfunction of the lacrimal apparatus causes the condition of dry eyes. The lacrimal glands can experience inflammation during instances of respiratory infection [46]. The nasolacrimal ducts also experience inflammation during respiratory infection. Since respiratory illnesses frequently transmit through aerosolized nasal droplets, the nasolacrimal ducts are examined in this thesis paper for catching respiratory illnesses. This can provide an early warning sign for infected individuals, which may not be exhibiting symptoms of a fever.

Inflammation is an autonomic response signaled by inflammatory cytokines. These are a type of biomolecule produced by immune cells and macrophages. They engage the immune system, cause inflammation, and create fever [9]. Their primary function is to coordinate the inflammatory response which is part of the body's defense mechanism. Zoukhri provides an overview of the lacrimal gland function and the effect of inflammation [46]. Secretions by the lacrimal glands are controlled through innervation by the parasympathetic and sympathetic nervous systems [46]. Several pathological conditions cause the immune system to target the lacrimal gland and create inflammation [46]. Sjogren's syndrome, sarcoidosis, graft versus host disease, and aging are all known to cause inflammation of the lacrimal gland [46]. Other conditions such as hepatitis C, Acquired Immunodeficiency Syndrome (AIDS), Human Immunodeficiency Virus (HIV), thyroid disease, and diabetes [46]. These inflammatory conditions disrupt tear secretions by the lacrimal glands and can result in dry eyes [46]. Inflammation of the lacrimal glands could interfere with remote temperature measurements of the eyelids. Abnormal amounts of tear production can also cause issues reading ocular surface temperature, due to changes in emissivity resulting from different tear film thicknesses.

Allergies are an obvious source of irritation and resulting inflammation of the nasolacrimal ducts. Nasal allergies are caused by irritants such as pollen, dust, and mold. Symptoms include itchy nose and eyes, sneezing, and runny nose. These can be difficult to discern from the initial symptoms of a common cold. The symptoms of allergies are caused by histamines. Histamines are biomolecules contained in some cells. Histamines trigger the allergic response to remove the substance from the body. Antihistamines are used to alleviate the symptoms of nasal allergies. For the nasolacrimal ducts to be useful in a diagnosis, additional markers will need to be considered.

2.9 Summary

Heat transfer is a fundamental property of passive temperature measurement. The three mechanisms of thermal energy transfer to consider are conduction, convection, and radiation. Sensors must arrive at thermal equilibrium to accurately detect the temperature of its environment. Historically, contact thermometers have used conduction to measure human body temperature. Convection is not considered to be an accurate form of temperature measurement, because it depends on too many variables resulting from environmental factors. Radiation is the chosen form of remote temperature measurement. IR cameras passively detect thermal radiation and therefore subvert the limitations of contact-based sensors. This is possible because all objects emit thermal radiation at temperatures above absolute zero. The measurement of infrared radiation is a function of a material's temperature and the emissivity of its surface area. Emissivity is the material property that governs the radiation of thermal energy from a surface.

Thermoregulation is a vital function of endotherms. Disruption in thermoregulatory processes can indicate an underlying physiological problem. Fever is produced by the human body to combat viral and bacterial infections. It is part of the natural immune response. Vasodilation and vasoconstriction are also responses of the autonomic system that regulate temperature. Observing blood flow through superficial vessels can lead to medical diagnosis. The lacrimal apparatus is examined as a possible source of heat-producing inflammation. The lacrimal ducts are susceptible to inflammation resulting from either allergies, blockage, or infection. Allergies and lacrimal duct blockages do not cause increases in HR and RR. This can provide a better indication of respiratory illness, compared to evaluating core body temperature alone.

Chapter 3: Hardware

Physical systems are constructed with hardware. A brief history illustrates that the success of thermal imagers depends on their resolution to cost ratio. Original thermal cameras were the product of Cold War research. They were constructed using a scanning-based design. Contemporary thermal cameras are high tech focal plane sensor arrays with proprietary mobile applications. The recent advances in consumer-based products have inspired a reevaluation of Infrared Thermography (IRT). The FLIR ONE Pro is one such consumer level device. It is commonly used by industry technicians for examining thermodynamics and diagnosing electrical problems. The wiring harnesses of modern automobiles have become too complicated to check by hand. The FLIR ONE Pro is used to check for bad connections by looking for hot spots. Medical researchers also appreciate the compact and intuitive nature of the FLIR ONE Pro. The attraction to this camera system is its ability to capture both thermal images and standard RGB photos. High cost and short battery life make the FLIR ONE Pro less desirable for our purposes.

The TOPDON TCView TC001 is instead selected for development purposes. The Windows compatible USB driver allows for python to access the video stream directly. Android compatibility provides a wide user base. Low power consumption allows the camera to operate for extended periods. Finally, the Raspberry Pi is evaluated for a low-cost alternative for building a kiosk-based product. The Raspberry Pi is a single board computer (SBC) for embedded Linux applications. It is becoming popular for medical researchers to provide portability. It is reviewed for its capabilities in running ML algorithms. It is ultimately chosen to provide a kiosk-based prototype.

3.1 History of Thermal Imagers

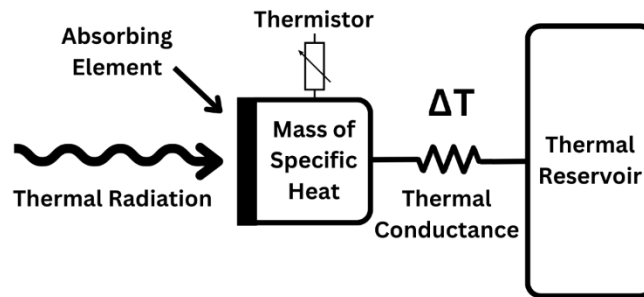


Figure 3.1: Conceptual diagram of a bolometer. Used for remotely detecting temperature.

Medical IRT is made possible through the development of high-quality infrared cameras. Ring discusses the history and advancement of medical IRT [38]. The bolometer was developed by American Professor, Samuel Langley, in 1878 [38]. A bolometer measures temperature remotely by absorbing radiant heat via a thin strip of an exposed conductor which is thermally coupled to a mass with known specific heat. The mass and specific heat of absorbing materials are required to calculate the temperature of an object that radiates thermal energy. A thermal reservoir is maintained at a known temperature to provide a reference. A known thermal conductance controls the rate at which thermal energy is transferred between the reservoir and absorbing mass. Thermal reservoirs can be maintained at either hot or cold temperatures [38]. A thermal conductance is placed between the mass and reservoir to maintain constant temperature in the absence of incident radiation. A thermistor measures the temperature of the mass. Thermistors are types of resistors whose electrical resistance is strongly correlated with temperature. Resistance is an electrical property of materials that is inverse to its ability to conduct current. Resistance is chosen as an electrical property to measure because its true value depends on temperature.

3.2 FLIR ONE Pro



Figure 3.2: Picture of FLIR ONE Pro thermal camera. This model has a USB-C port for compatibility with Android mobile devices.

The FLIR ONE Pro is a 3rd generation thermal camera attachment designed for use with mobile phones. It is available for both Android and iOS. The FLIR ONE Pro has two camera sensors built in. The IR camera operates in the 8-14 μm range and has a resolution of 160 x 120 pixels. The visual camera has a resolution of 1440 x 1080 pixels. It is capable of measuring temperatures from -20 C to 400 C with a sensitivity of 70 mK. An onboard battery prevents power drain from the mobile device but needs to be recharged separately. This third generation of FLIR thermal imaging systems is advertised to be more advanced than previous models [14]. The new OneFitTM feature allows the USB-C port to be adjusted in height so that it does not impact the mobile phone case [14]. Patented Multi-Spectral Dynamic Imaging (MSX[®]) technology provides more useful images by combining visible-light contours with the thermal image. The MSX[®] distance is adjustable from 0.3 meters. Other FLIR products include the FLIR DuoTM, a light-weight version suitable for drones [14]. The FLIR C3 is a pocket-sized version complete with a 3-inch touchscreen and Wi-Fi connectivity [14]. Proprietary mobile apps for Android and iOS provide color palettes and temperature spot measurements.

Thermal cameras like the FLIR ONE Pro have numerous applications across multiple industries. They are excellent for contributing educational value to science classes. Electrical companies can use thermal cameras to monitor the power lines. Firefighters can use them to detect hot spots and monitor forest fires. Search and rescue operations can deploy thermal cameras to find survivors. The military use thermal cameras to find targets at night. Police use thermal cameras to find perpetrators hiding in the dark. Drones and helicopters can be used to carry thermal cameras further than before. Diagnosing electrical problems is an increasingly difficult problem with contemporary technology. As the reliance on computer components increase, so do the number of fuses and wire harnesses required for power and control. Excessive electrical current or high contact resistance can both create hot spots in thermal scenes. This makes thermography a useful tool for technicians, to increase the speed and accuracy of diagnosing electrical problems.

Sara Scullin edited a review of the FLIR ONE Pro Thermal Camera by an automotive technician [15]. Typically, automotive technicians are required to disassemble the fuse box and wire harness, to check each component for voltage drops [15]. It quickly becomes difficult to locate and diagnose electrical problems without a remote diagnostic tool. By using a thermal camera, the fuse box and wire harness can be checked for temperature gradients indicating current leakage [15]. IRT can help locate problems faster and more accurately. The FLIR ONE Pro mobile app allows technicians to show the problem to their customers. The solution can then be verified by taking follow up pictures after the fix was completed [15]. The proprietary technology provides a professional presentation for technicians. Thermal cameras such as the FLIR ONE Pro provide inexpensive tools to view the radiation of thermal energy. This can illustrate asymmetries which are the result of a defect or abnormality.

Kirimtat et al compare the use of FLIR ONE Pro and SEEK Compact Pro thermal cameras for medical diagnostic purposes [24]. The FLIR ONE Pro is used more frequently for research in biomedical diagnosis, because the MSX[®] feature provides more detailed information by combining visible light features with thermal images [24]. A limitation of MSX[®] technology is the requirement of maintaining preset distances to the object. This ensures the RGB and thermal images align properly. Failure to align the two images produces a second contour in the MSX[®] image, which can mimic the appearance of noise [24]. Unlike the SEEK Compact PRO, the FLIR ONE Pro uses proprietary image formats in the app database [24]. Images can only be used for processing outside the FLIR Android app environment after exporting the desired image. They also note that the FLIR ONE contains an internal battery, which requires frequent recharging [24]. The onboard battery is required for heating a thermal reservoir. This provides another limiting factor for thermal monitoring applications requiring extended runtime. Although pass-through charging allows this FLIR ONE Pro to operate for extended periods of time, it also requires an unsightly power cord.

The FLIR ONE Pro version with USB-C for Android was used in initial tests. The proprietary MSX[®] feature of the FLIR ONE Pro makes it attractive to consumers for numerous applications. Unfortunately, the MSX[®] feature did not provide enough information for standard facial landmark detection. These FLIR products do not provide the USB compatibility for open-source tools. Users are forced to rely on the sole features of a few mobile apps to utilize thermal imaging in their workflow. Developers are required to request access to the official Software Development Kit (SDK). Also called devkits, SDKs provide software-building tools for a specific product. The FLIR ONE Pro is best suited for technicians and hobbyists looking to acquire standard and IR images with the features provided by the proprietary mobile apps.

3.3 TOPDON TCView TC001



Figure 3.3: Picture of TOPDON TCView TC001 thermal camera. This thermal camera is compatible with Android and Windows.

The TCView TC001 by TOPDON is a consumer level IR camera with an IR resolution of 256x192 pixels [43]. This is an improvement over the resolution of a FLIR ONE Pro. It is advertised to produce thermal images with excellent clarity, where the difference of surface temperatures is minimal [43]. It can function in a wide range of conditions, and measure temperatures between -20°C and 550°C [43]. Temperature measurements are rated to an accuracy of 0.1°C [43]. It has a low power consumption of only 0.25 Watts [43].

The TCView TC001 is suitable for extended usage on Android mobile devices. It is not currently available for IOS. The Android mobile app is useful for visual and educational purposes. There is a Windows app that makes thermal imaging available on a personal computer (PC). The availability for use on Windows suggests the use of compatible USB drivers. This is generic enough to make the sensor camera image available for open-source programming languages like Python. They are also usable by the Linux OS found on Raspberry Pi, discussed subsequently. Implementing Computer Vision (CV) requires the ability to read the thermal image stream directly from the USB port. We utilize this unintentional feature for using the thermal video stream outside the proprietary mobile app.

The low-cost and open-source nature of Raspberry Pi computers makes them attractive to software researchers and product developers. Hosny et al created a program to accept either a CT scan or X-ray of the chest, analyze the image, and subsequently diagnose Covid-19 [20]. This demonstrates the ability of embedded Linux platforms, like the Raspberry Pi, to create medical diagnosis. This was previously accomplished using DL algorithms, which require too much computational power to make them portable and affordable [20]. Instead, Hosny et al used Local Binary Patterns (LBPs) and multichannel fractional-order Legendre-Fourier moments to identify local and global features, respectively [20]. The images were classified by removing noise and other features that do not pertain to the diagnosis [20]. The final trained image classifier model was only 3 MB and achieved similar accuracy as the full DL models [20]. By taking time to make the computer algorithms more efficient, hardware dependencies were reduced.

An available ribbon style camera and USB ports provide two different methods of attaching a camera to the Raspberry Pi. This makes it attractive for Computer Vision (CV) applications. Abdulhamid et al demonstrate CV on the Raspberry Pi by implementing object detection with Python [1]. Python and OpenCV were chosen as the programming frameworks, due to their compatibility with Raspberry Pi [1]. These programs will be discussed further in Chapter 6. A Gaussian blur function is applied to reduce noise on the color images [1]. Then, Canny edge detection algorithm was used to find the boundaries [1]. Morphological transformation was employed to close any open spaces along the detected edges [1]. A Contour approximation was then applied to the edges [1]. Contours are curves that connect points. They are used to save resources during object detection by approximating the edges [1]. Results of this object detection indicate an average efficiency of 90.2% [1]. This illustrates the capability of utilizing Raspberry Pi for real-time computer vision applications.

3.5 Summary

Infrared thermography has a long history which unfolded as the technology behind thermal cameras improved. Originally, thermal imagers for medical purposes were of a scanning-based design [35]. Low resolution, framerate, and dependency on liquid nitrogen for coolant reduced the accuracy and reliability of medical IRT. This project evaluates the use of two different thermal cameras for two different reasons. The FLIR ONE Pro was initially selected for its dual camera functionality and proprietary MSX[®] technology. It has been demonstrated by technicians at diagnosing short circuits and corroded contacts. It is commonly chosen by medical researchers for studying disease. Several reasons made the FLIR ONE Pro a poor choice for our purpose. The FLIR ONE Pro has lower IR resolution than comparably priced thermal cameras. Also, an internal battery powers a thermal reservoir which limits runtime and requires frequent recharging. Difficulty accessing the USB port directly via Python reduces the number of possibilities for developers.

The TOPDON TCView TC001 was chosen for the development of this thesis project. It has a higher resolution than the FLIR ONE Pro, making it a better choice for acquiring clear IR images. Lower power consumption and no internal battery allow the TCView thermal camera to operate for extended periods on mobile devices. The Windows compatibility provides the USB drivers required for accessing the sensor data directly. Raspberry Pi was selected to make a kiosk-based version of the device. It is an embedded Linux device with similar computing power to a low-end laptop. This SBC has been demonstrated as an affordable alternative to running ML algorithms on more power intensive devices. The open-source nature of Raspberry Pi computing means there are more compatible libraries and demonstrative projects with which to immediately begin developing.

Chapter 4: Medical IRT

This chapter reviews some of the medical applications of Infrared thermography (IRT). IRT has a rich history that begins with the study of breast cancer. The fast growth of tumors requires increased consumption of nutrients compared to surrounding tissues. It also creates a physical anomaly within the anatomical structure. The increase of blood flow and metabolic activity results in asymmetrical temperature differentials that can be observed from thermal images. Thermal cameras are also being used to evaluate the severity and healing potential of burn wounds. Burnt skin has nearly the same emissivity as healthy skin. Thermal cameras can be used to evaluate the healing potential and assess the need for skin grafts. The healing of broken bones can be observed via thermal cameras. The metabolic process of healing generates significant heat. The resulting temperature differential can be used to determine the percentage of the bone that has healed, without the need for multiple X-Ray images. Complex Regional Pain Syndrome (CRPS) is difficult to diagnose and treat, but here thermal imaging cameras also play a role. Focal infections are one of the most difficult conditions to diagnose. As pockets of bacteria that are walled-off from the rest of the body, they are frequently undetected by conventional medicine. But metabolic activity cannot hide from thermal imagers. Focal infections are detected by finding hot spots on thermal images. Hot spots are not indicative of thermal equilibrium. Only because the emissivity of thermal radiation exceeds the diffusivity of tissues, can the temperature differential be detected. This will limit detection to the surface regions. In these cases, IRT locates the asymmetrical temperature differentials associated with disease.

4.1 History of Thermography

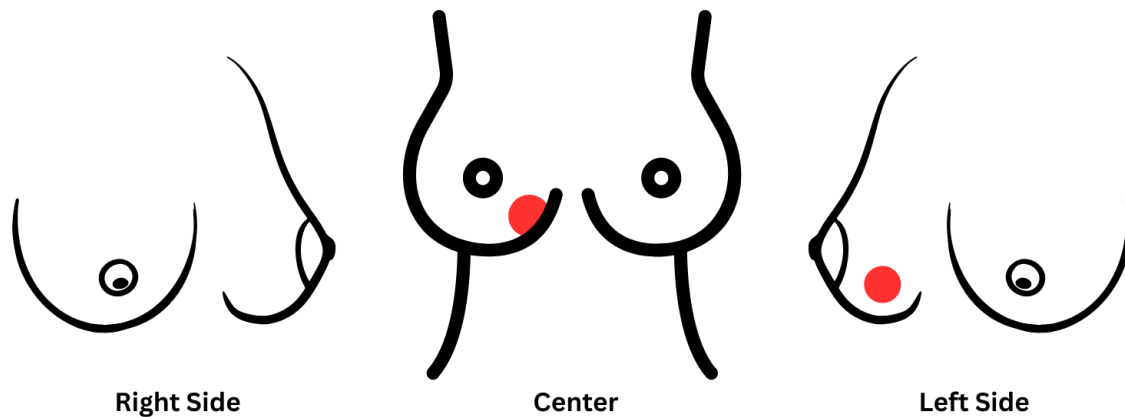


Figure 4.1: IRT diagram of female breast demonstrating a cancerous lesion. Note that the lesion is not visible from every angle, so care should be taken to image the entire breast region. Modified from [16] [26] [39].

Breast cancer is one of the most extensively studied diseases using infrared thermography. Fraser provides a brief historical perspective of breast thermography in Canadian medicine [16]. In the early 1950s, Dr. Ray Newton Lawson discovered that breast tumors produced more heat than the rest of the body [16]. This results in a temperature differential between 1.75 and 3.5 degrees between a malignant tumor and the surrounding breast tissues [16]. In 1956, Dr. Lawson started experimenting with the Baird Evapograph, an early infrared imager that was originally developed for Cold War military defense [16]. Thermography was recognized by the medical community as a new “method of medical imaging that had the potential to revolutionize the field of cancer screening by allowing doctors to see what no health care professional had ever seen before” [16]. By 2012, Canadian health officials declared that “thermography would no longer be considered a viable method of screening Canadian women for breast cancer” [16]. The medical community now argue that medical thermography is dangerous since it is not effective [16].

Tumor formation requires additional oxygen and nutrients to sustain increased metabolic activity in focal regions. This is provided by blood which also carries core body heat. When close enough to the surface of the skin, temperature differentials can be detected by thermal camera [26]. Kontos et al noted that thermography was explored in the 1970s and 1980s but disregarded due to poor performance [26]. A Meditherm med2000 thermal imaging system was utilized to detect breast cancer [26]. Materials and methods used in this study indicate that digital infrared thermal imaging (DITI) provides low sensitivity in the detection of breast cancer [26].

Sarigoz et al evaluate the use of Digital Infrared Thermal Imaging (DITI) to diagnose breast lesions [39]. For the double-blind study they used the FLIR ThermaCam E45 [39]. They found measurable differences in the temperature patterns found in different types of breast lesions. These differences were discernible between benign cysts and malignant tumors, but not between ductal carcinoma and granulomatous mastitis [39]. The difference between benign and malignant tumors is significant due to the danger of metastasizing. Once a malignant tumor has been discovered, conventional medical techniques can be used to determine the type of cancer.

The rounded surface of breasts makes it more difficult to use imaging techniques. Conventional mammograms compress the breast into a flat shape for 2-dimensional imaging. X-rays are used because cancer is denser than fat. Therefore, tumors appear as light or bright spots on a mammogram. Compression can restrict blood flow and disrupt thermoregulation. The disruption of thermoregulation could potentially skew medical IRT results. It is important in IRT to take measurements that are normal to the surface. Measurements taken at angles greater than 45 degrees will not express the same emissivity. Therefore, it is important to take IR photographs from enough angles to visualize the entire breast surface without compression. This enables the use of IRT to map temperature differentials across a curved surface.

4.2 Burn Wounds

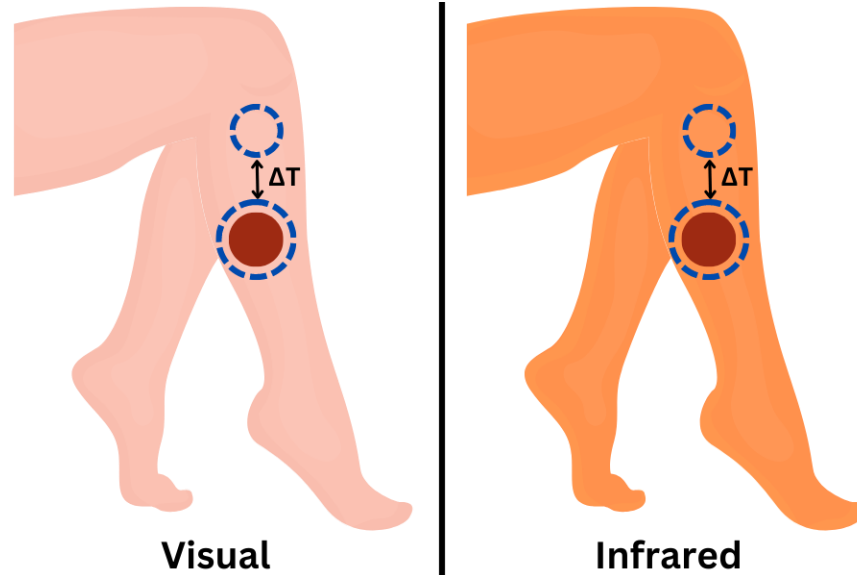


Figure 4.2: Multispectral diagram illustrating the analysis of burn wounds. The visual and infrared spectrums are utilized. Modified from [21].

Histological analysis of burn wounds is commonly used to determine the severity of a burn. It requires a biopsy and therefore only examines a small piece of the wounded tissue. Laser Doppler Imaging (LDI) could be an effective tool, but only between days 2 through 5 after a burn injury [21]. Jaspers et al conduct a reliability study to determine the effectiveness of using the FLIR ONE thermal imager to examine the severity of burn wounds [21]. The proprietary mobile app was used to compare average temperatures of burned and normal tissues. Circles were drawn in the visual spectrum and temperatures measured in the infrared spectrum. This allows for easier manual annotation of the ROI. The comparison of temperatures averaged from adjacent regions can provide a more reliable measurement system. Burn injuries were categorized by the amount of time required to heal [21]. Healing was determined when the skin had regained at least 95% of the epithelial layer [21]. User error was determined by correlating measurements taken by two different observers and found to be within acceptable limits [21].

4.3 Broken Bones



Figure 4.3: IRT diagram of distal forearm fracture healing. Modified from [5].

Ćurković et al conduct a study to observe the temperature difference in pediatric forearm distal fractures during the healing process [5]. The study was conducted on otherwise healthy children between the ages of 4 and 14 years. They took thermal and X-ray images every 7 days between 1 and 4 weeks after the injury [5]. The highest temperature differential was found to be 2 degrees Celsius at week 1. This represents the period when the healing process is generating the most heat. The lowest temperature difference of 0 degrees Celsius was found at weeks 3 and 4, after the fracture had healed [5]. After the bones had healed, thermoregulation returned to baseline. This is highly suggestive of the correlation between healing processes and measurable skin temperature [5]. Metabolic processes of cell division consume energy and burn calories. The metabolic processes generate heat through catabolism. Additionally, increased blood flow is required to deliver the additional nutrients. The combination generates a temperature differential between normal and healing tissues. Thermal imagers can therefore be used to monitor the healing process without subjecting patients to subsequent X-ray radiation.

4.4 Complex Regional Pain Syndrome

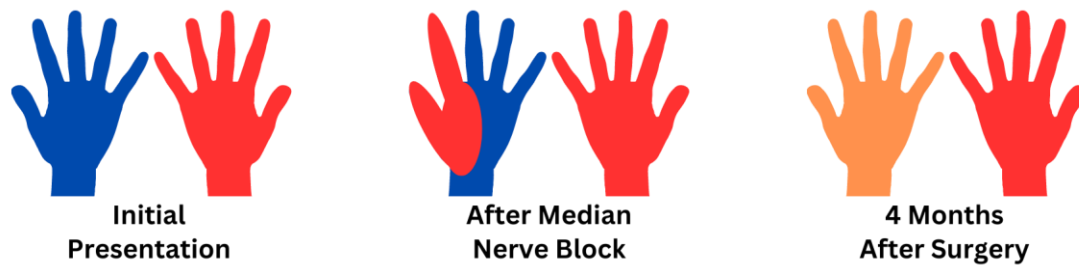


Figure 4.4: IRT diagram illustrating the healing process of CRPS. Modified from [7].

Dhatt et al conducted a small case study to examine the use of a FLIR ONE imager to diagnose and monitor the treatment of Complex Regional Pain Syndrome (CRPS). CRPS is characterized by pain, thermal asymmetry, and loss of function in an arm or leg [7]. It can be caused by trauma to one of the appendages, such as being crushed or fractured. Inflammation causes the nerves to be more sensitive than normal, and this can result in permanent damage long after the injury has healed. CRPS is diagnosed by excluding conditions with similar symptoms, such as rheumatoid arthritis. A quick and accurate diagnosis is essential because the timely restoration of blood flow is vital to preventing permanent damage. It is treated with prednisone and if necessary, with corrective or decompressive surgery. Dhatt et al use the FLIR ONE system to monitor temperature asymmetry as a patient with CRPS improves. Healing is achieved when the cold hand returns to normal temperature. In some cases, a Diagnostic Anesthetic Nerve Block (DNB) is used to assess the pain distribution. A decrease in pain and warming sensation are reported almost immediately. This provides the evidence and location for corrective surgery [7]. Once the affected areas are identified, corrective surgery can be attempted. Complete recovery is possible when diagnosed and treated accordingly.

4.5 Focal Infections

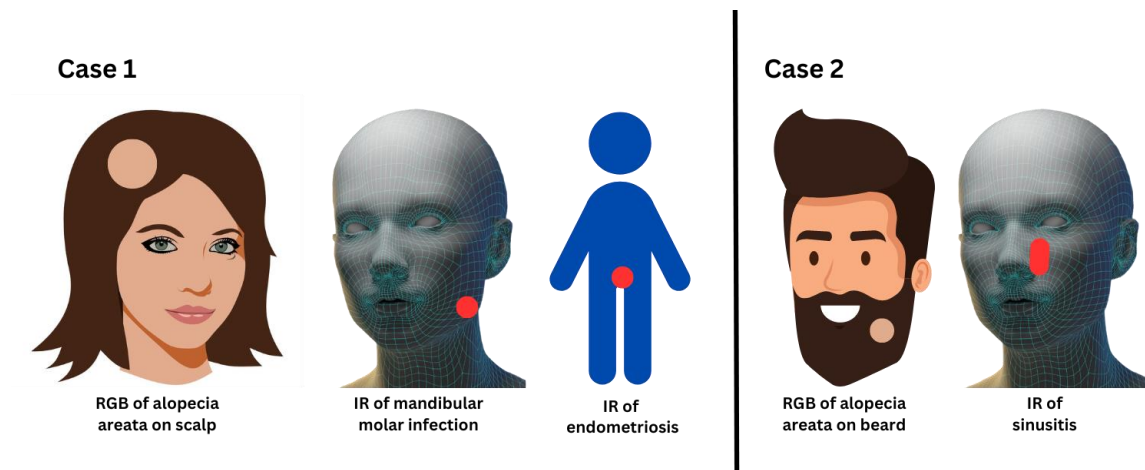


Figure 4.5: Diagram illustrating the use of IRT to find hidden focal infections. Modified from [18].

Focal infections are pathological conditions caused by a virus or bacteria that is contained or restricted to a localized region. They are difficult to detect, because the infection is enclosed within a wall of defensive tissue [18]. In these instances, blood tests are usually negative for antibodies because the body is not actively fighting the infection. Grozdanova-Uzunova discuss two case studies in which IRT was used to diagnose hidden focal infections [18]. In both cases, the only symptom was alopecia areata of the scalp or beard respectively [18]. Alopecia areata is a condition characterized by hair loss in a localized region. The FLIR T334 thermal imaging system was utilized, with a thermal sensitivity of 0.05 degrees Celsius and resolution of 320 x 240 pixels [18]. Endometriosis and a molar infection were diagnosed in the first case study by finding the areas of highest temperature [18]. The second case study revealed a sinus infection through the same method [18]. Thermal images of healthy people demonstrate a high degree of symmetry across the vertical axis of the face. A temperature differential of 0.4 degree Celsius may indicate disease [18]. By finding asymmetrical hot spots on the surface of the skin, we can find hidden focal infections.

4.6 Summary

The importance of temperature in medicine has been well understood for a long time. The ability to accurately measure temperature was always a limiting factor in the development of thermography. The long history of medical IRT begins with breast cancer. Early successes and failures with medical IRT have largely dissuaded the medical community from further pursuing the technology. Now, improvements to thermal imaging systems have spawned new areas of research into medical IRT. New focal plane thermistors increase the number of temperature measurement points, therefore providing significantly more information than a single scanning thermistor.

Several medical conditions have been successfully diagnosed from thermal images. These include the analysis of burnt skin for determining the need for grafts. Medical IRT is also used to monitor healing over the course of treatment for broken bones and CRPS. Focal infections prove difficult to locate by conventional means. Pathology tests and broad-spectrum antibiotics don't work in these cases but are easily identified as hot spots on IR images.

Several temperature asymmetries have been attributed to diagnosed medical conditions. Temperature differentials as low as 0.4°C can indicate the presence of an underlying disease. Some of these ailments are difficult to diagnose or treat using conventional methods. The references in this chapter all illustrate that IRT can be used to provide accurate diagnosis and monitoring of medical conditions. As hardware and software tools continue to advance, it is inevitable that the medical community returns to the use of IRT for non-invasive diagnostic purposes. The rise of smaller, more affordable thermal cameras and advanced software packages can help bridge the gap between hospitals and patients. This will serve to reduce the time, risk, and cost associated with frequent medical testing.

Chapter 5: Related Work

Remote fever detection and the diagnosis of respiratory illness is currently a hot topic for medical IRT. Similar research points out the problems and implications of detecting fever by measuring the center forehead. As previously mentioned, more accurate core body temperature measurements are obtained by measuring the lacrimal caruncles, or inner canthus of the eye. A difference of 0.55°C between the lacrimal caruncles and center forehead provides an early warning for URTIs.

Comparing the core body temperature with that of the peripheral body temperature provides a unique method of triaging Emergency Room (ER) patients. They are placed into categories based on stability. Patients that are relatively healthy and stable will have greater temperature differentials measured between the lacrimal caruncles and tip of the nose. Low peripheral body temperature can signal the risk of sudden deterioration in ER patients.

Measuring body temperature is not enough to infer the presence of a disease. Variables such as stress, exercise, and environmental conditions can also affect body temperature. Heart Rate (HR) and Respiration Rate (RR) can be measured remotely using both visual and thermal cameras. The remote measurement of vital signs is important for the continuous and noninvasive monitoring of patients. This type of dynamic measurement elicits the use of video streaming. Previous works relied on processing images. Adding the vital signs into a diagnostic metric can improve the accuracy of medical IRT. It is less likely that a person's breathing and heart rate are elevated with core body temperature. This assumes that the patient has had enough time to relax and reach thermal equilibrium.

5.1 Acute Respiratory Illness

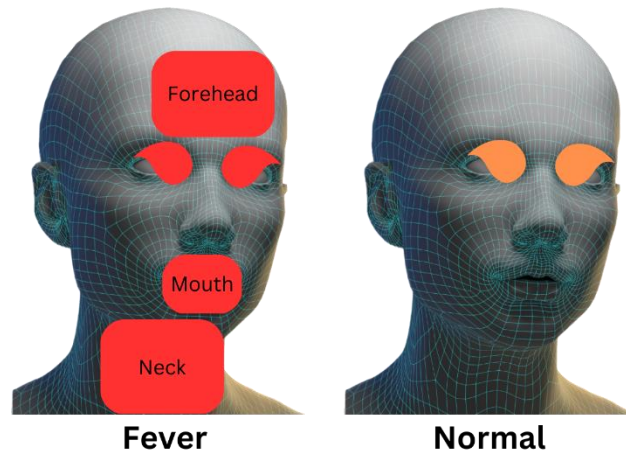


Figure 5.1: IRT diagram of face illustrating fever and normal conditions. Modified from [45].

Zuopeng Zhang et al evaluate the use of infrared thermography on patients with acute upper respiratory tract infection [45]. They utilized an ATIR-M301B far-infrared thermal imager for taking thermal images [45]. The ATIR-M301B is an uncooled focal plane digital thermal imaging device with an impressive temperature resolution of 0.05°C [45]. Zuopeng Zhang et al conclude that acute respiratory illness can raise the core body temperature and create hotter regions around the throat and nasal cavities [45]. Infrared thermography can show these abnormal temperature differences on the surface of the skin indicating an underlying pathological condition [45]. Figure 5.1 illustrates the temperature patterns of a patient in an advanced stage of fever. A common problem with medical IRT results is to represent healthy and infected cases using different pseudo color palettes. While this creates greater visual effect, it does not help with accurate interpretation. Comparing thermal images represented with different pseudo color palettes is akin to comparing apples to oranges. The pseudo color palettes are artistic but not quantitative. To compare temperature differences represented by color, the color palettes and calibration scales should be identical.

5.2 Covid-19

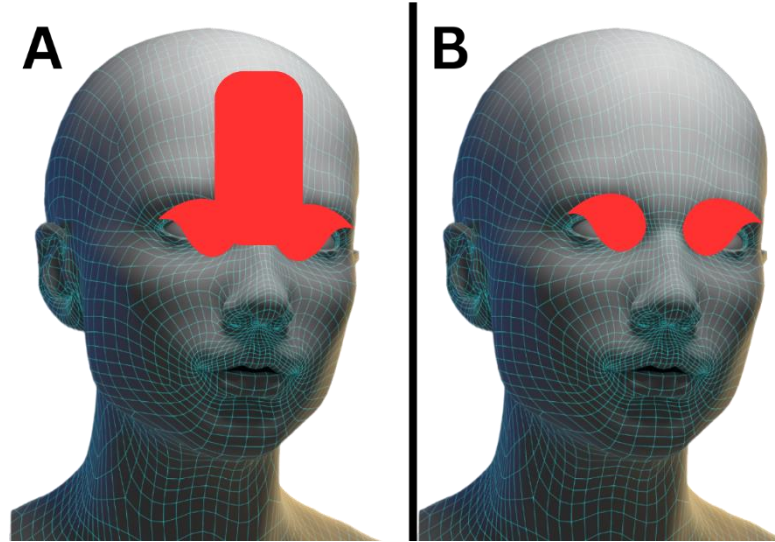


Figure 5.2: IRT diagram of healthy patient (A) compared to patient with Covid-19 (B). Note the temperature difference between the lacrimal caruncles and center forehead. Modified from [29].

Martinez-Jimenez et al performed a study to evaluate the use of infrared thermography for the diagnosis of pre-symptomatic Covid-19. They found that a temperature difference between the lacrimal caruncles and center forehead is indicative of Covid-19 infection [29]. 82% accuracy was obtained when the temperature difference was greater than or equal to 0.55°C [29]. This study illustrates that measurement of the center forehead temperature alone is not enough to diagnose pre-symptomatic cases of Covid-19 infection. This important research combats the current practice in fever screening of measuring center forehead temperature. The background information discussed in chapter 2 suggests that this result is more likely to represent generic URTIs than a specific indicator of Covid-19 infection. Subsequent articles further demonstrate the use of core body temperature readings from the ROIs otherwise known as the lacrimal caruncles. Diet, exercise, time of day, stress levels, and environmental factors also play key roles in the thermoregulation of core body temperature. Core body temperature alone can be affected by too many variables to be considered a proof positive indicator of contagious diseases.

5.3 ER Triage

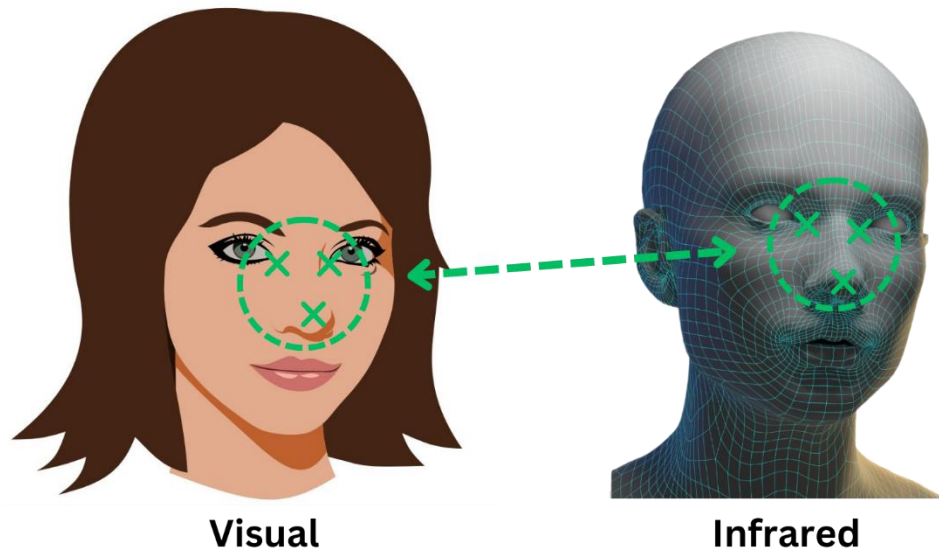


Figure 5.3: Core vs peripheral body temperature measurements. A homography matrix is used to translate the coordinate points from the visual to infrared images. Modified from [2].

The idea of Baskaran et al, is to measure the difference in temperature between the lateral caruncles and the nasal tip [2]. If the difference is significant, it can show that blood flow has been restricted to the vital organs. This demonstrates that the patient is in danger of rapid deterioration. The problem they encountered, is that it takes too long to manually measure and record the temperature differentials as part of the Emergency Room (ER) admittance routine [2]. They solve the problem by creating a thermal image application to measure the temperature differential [2]. They used a FLIR ONE Pro because of the dual cameras. An app provides a template to align the face with the ROIs in the visual spectrum. The lacrimal caruncles are identified as the hottest points and used to align the thermal and visual images. This technique subverts the need for more extensive deep learning models to provide landmark annotation. It does require additional cooperation from the app users. The measured temperature differential provides a gradient which is used by the doctors to aid in triaging patients.

5.4 Remote Heart Rate

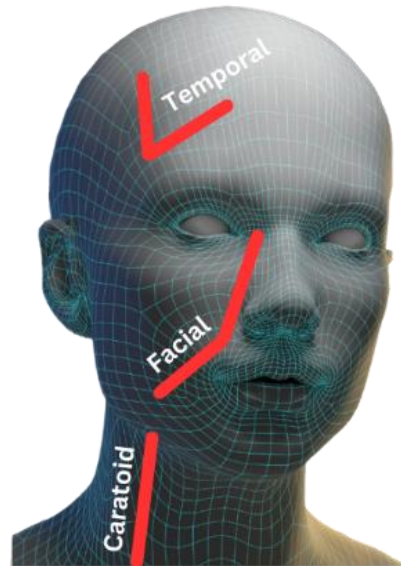


Figure 5.4: Superficial arteries of the face and neck. Approximated on a mask for anatomical clarity. Modified from [17].

A beating heart sends warm blood through the arterial system as an important aspect of thermoregulation. The diffusivity of skin provides a dynamic response to the cardiac rhythm. Heart Rate can be detected remotely in either visual or infrared spectrums. This is a dynamic measurement requiring the use of video analysis. Previous diagnoses were attained by reading still images. Garbey et al discuss Heart Rate (HR) measurement devices and principles [17]. Previous methods include Electrocardiography (ECG), piezo-electric pressure sensors, doppler ultrasound, photoplethysmography, and laser doppler [17]. These all require either physical contact with the patient, or using a form of radiation, whether by ultrasound wave or laser [17]. It is important to develop reliable methods to remotely detect heart rate without interfering with the patient or requiring their participation.

Garbey et al created a new method for remotely sensing Heart Rate (HR) via passive thermal imaging system [17]. They use a MWIR camera with a temperature resolution less than

25 mK and spatial resolution of 640 x 480 pixels [17]. Superficial blood vessels in the neck or temporal region were selected due to the proximity to the surface and the likelihood of being exposed [17]. Other superficial arteries could be used depending on the angle of exposure. Garbey et al manually annotate a straight-line segment over a superficial artery and use motion tracking to account for slight movements [17]. Pixels are averaged over the x-dimension to reduce noise and create a 2-dimensional matrix, $A'(y, t)$ [17]. Power spectra is calculated by applying the Fast Fourier Transform (FFT) [17]. Power spectra is averaged using an adaptive line enhancement type method [17].

Poh et al note the physiological property of Blood Volume Pulse (BVP), which corresponds to the pressure wave resulting from a cardiac pulse [33]. As pressure changes in blood vessels beneath the skin, the path length of incident light changes measurably [33]. Using this principle, Poh et al create a new method of remote vital signs measurement using a simple laptop equipped with a standard RGB webcam [33]. They capture one-minute videos from willing participants, positioned half a meter away from the camera [33]. The camera recorded in 24-bit RGB at 15 fps and a resolution of 640 x 480 pixels [33]. Face detection was performed, and the bounding box was used to create a Region of Interest (ROI) [33]. The video was separated into RGB color channels for Independent Component Analysis (ICA) [33]. Custom MATLAB software was used to obtain the Blood Volume Pulse (BVP) [33]. Their results are strongly correlated with measurements recorded via traditional methods, using a finger-clip style BVP sensor and chest-belt style RR sensor [33]. This study supports the inclusion of RGB video processing in conjunction with IR video processing, to improve the accuracy and reliability of passive remote diagnostic systems.

5.5 Remote Respiration Rate

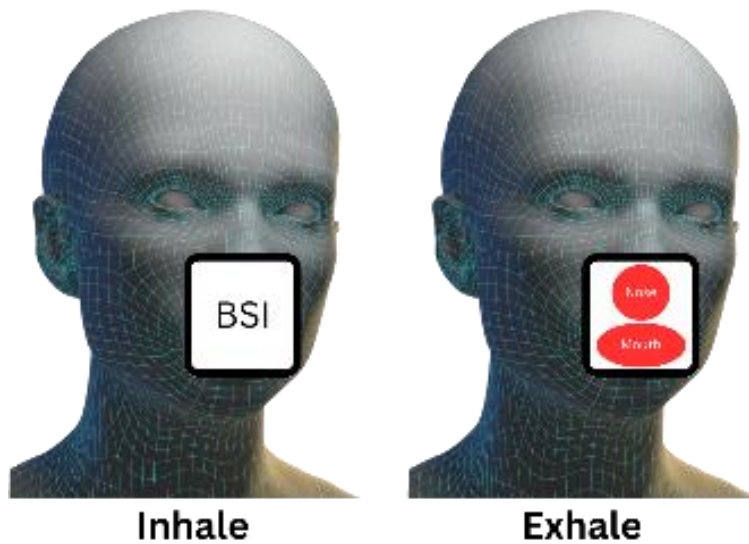


Figure 5.5: IRT diagram of remote RR with a BSI. A breathing sorption indicator (BSI) absorbs and evaporates the heat from respiration. Modified from [44].

Respiration is also an important part of the thermoregulatory process of endotherms. Panting, or breathing through the mouth, is used by mammals to keep cool. Heat is lost through the lungs due to the mechanisms of thermal energy transfer. Cool air is brought back into the lungs to replenish oxygen. This process is easily observed via thermal camera. Exhalation releases heat around the nose and mouth while inhalation cools these regions. Evaporation from condensed moisture and forced convection from inhalation cause the cooling effects.

Fei et al create a remote Respiration Rate (RR) measurement system with a passive thermal imaging camera [10]. They used a relatively elaborate FLIR SC6000 for the experiment [10]. The indium antimonite (InSb) sensor achieves a sensitivity of 0.025 degrees Celsius at a resolution of 640-512 pixels [10]. The relatively cool edges surrounding the nostril openings were selected as a boundary condition to monitor respiration [10]. A coalitional tracking method was implemented to compensate for patient movements during the RR measurements [10]. Fast

Fourier transform was applied to filter noise and detect the frequency of respiration. To filter noise, frequencies detected outside the range of normal breathing were ignored. The remaining frequency with the highest amplitude correlates well with RR measured with conventional means. Their results indicate that less expensive thermal cameras should be able to perform adequately, with lower thermal sensitivity and spatial resolution [10]. The major challenge is accurately tracking the ROI in thermal video. It must remain tracking long enough to average several breathes for accuracy.

Boris Vainer creates a more robust technique for measuring respiration waveform with IRT in humans and animals. The method, referred to as Sorption Enhanced Infrared Thermography (SEIRT), was able to acquire the respiratory waveform, with a high signal-to-noise ratio [44]. The approach is novel due to the use of a gauze-like cloth, called a Breathing Sorption Indicator (BSI), placed over or near the airway opening [44]. The BSI serves to capture and release the heat associated with respiration. It provides a significantly larger surface area than the nostril edges for enhanced detection of the breathing waveform. Almost any cloth can be used to function as a BSI. For the best results, the BSI material should have low specific heat and high emissivity [44]. Low specific heat allows the material to heat up and cool down quickly. As discussed in chapter 2, increasing emissivity increases the amount of thermal radiation being emitted from a surface. This improves the chances of accurate measurement. Slight movements by the patient are less likely to disrupt RR measurements with the BSI technique. Tracking is not necessary when the BSI and thermal camera can remain stationary. In this case, slight movements of the patient are irrelevant. Vainer notes that the actual temperature of BSI is inconsequential to the measurement of respiratory waveform [44]. Here is an example of relative temperature measurements being used to quantify vital signs.

5.6 Remote Vital Signs

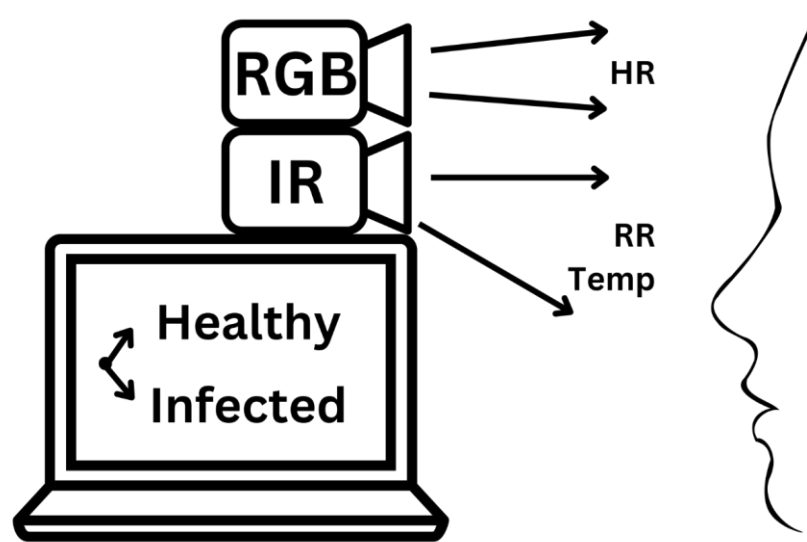


Figure 5.6: Diagram of RGB and IR cameras measuring vital signs. HR, RR, and core body temperature are used to detect influenza. Modified from [31].

Negishi et al point out that while IRT has been demonstrated to accurately measure body temperature, this type of fever screening can only provide a positive prediction 3.5%-65.4% of the time [31]. Simple fever screening does not provide enough information to reliably detect contagious respiratory illness and is not effective at controlling pandemic outbreaks [31].

Negishi et al created a new method to remotely detect the presence of influenza-like illness [31]. They combine the measurement of three vital signs, Heart Rate (HR), Respiratory Rate (RR), and core body temperature [31]. RR measurement was performed using IRT video. This requires a tracking mechanism for nose and mouth regions [31]. They used existing Dlib libraries on the RGB video and translate the coordinates to the thermal image via a homography matrix [31]. HR was acquired using the standard video. This involved splitting the standard video into RGB components for independent analysis. The combination of vital signs with core body temperature provides more accurate remote detection of influenza than temperature alone.

5.7 Summary

Similar previous works include using IRT to remotely diagnose acute respiratory diseases. It is apparent that core body temperature readings need to be taken from the lacrimal caruncles, with at least 9 pixels of resolution per each. The difference in this core body temperature and the center forehead can be indicative of pre-symptomatic respiratory illnesses. The peripheral body temperature can be estimated by measuring the tip of the nose. Baskaran et al found that if a difference in temperature between the core and peripheral body temperatures exceeded a threshold value, ER patients were at an increased risk of sudden deterioration. This is important for medical triage, to quickly categorize the stability of a patient.

Vital signs such as HR and RR have been demonstrated measurable by RGB and IRT videos. HR is determined by taking the FFT of a linearized segment of pixels that correspond to a cutaneous location above a superficial artery. RR can be found by examining dynamic temperature response in and around the mouth and nostril ROIs. In humans, breathing is a mechanism of heat and gas exchange with the environment. Therefore, IRT can be used to detect the waveform. FFT is used to determine RR from the breath waveform. Respiration waveform measurements can be improved with the addition of a BSI.

These previous works best illustrate that combining the vital signs measurement with core body temperature provides more information and can increase the accuracy of a remote diagnosis for respiratory illnesses. This is because too many factors can influence the core body temperature alone. In the presence of respiratory infection, HR and RR are also likely to be increased. It can be reasonably expected that HR and RR will decrease before core body temperature in the event of physical exertion or excessive ambient temperatures.

Chapter 6: Application Software

Now that we understand some of the medical applications of IRT, we require the software to construct a secure application. By the end of this chapter, we will have built the foundational basis for an enterprise grade streaming server. Web applications require methods to securely host services on the internet. We start by discussing nginx as a web server for reverse proxy. This provides a robust method to route traffic between the world wide web and our developmental servers. Then we discuss open-source TLS certifications by adding Certbot to our nginx server. This enables encrypted traffic and provides 3rd party authentication. Streaming videos is a well-developed and robust process, so an RTMP server is subsequently added to nginx. Python is the primary programming language for dealing with high-level math related to image processing. It provides access to numerous computer vision libraries. OpenCV is one such library. It is used to analyze each frame to calculate various Regions of Interest (ROIs) and provide a diagnosis via annotating video frames. Augmented reality results from combining the multispectral data between RGB and IR cameras. Flask is the Python based server framework that handles client requests. It listens for requests and spawns the OpenCV process. Flask must release the frame lock to ship a video stream. Accessing videos on the world wide web elicits the need for security. Many websites do not take measures to protect static content such as images and video. A JavaScript method of authentication is described utilizing JSON Web Tokens (JWTs). Finally, the heavy cost of bandwidth using MJPEG streaming is identified, and a solution is proposed. Images contain a lot of information that does not change between frames. Video streams save bandwidth by instead tracking the differences between frames.

6.1 Nginx

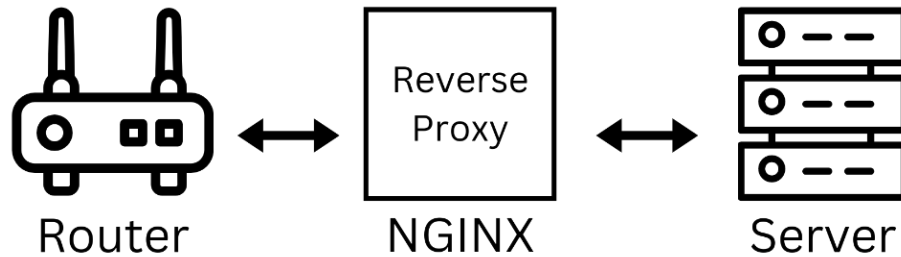


Figure 6.1: Block diagram illustrating the use of nginx as a reverse proxy.

Initially released in 2004, nginx is a fast and lightweight web server widely used today. It excels in handling reverse proxies, static images, and RTMP video streaming. Rather than threads, it utilizes an approach that is asynchronous and event driven. Asynchronous means that server requests and responses do not have to be handled in turn. This makes it highly efficient for handling web traffic. It's commonly deployed in front of developmental servers as a reverse proxy. This adds security and scalability. We are to use nginx for its reverse proxy, TLS, and RTMP functionalities. The nginx software runs best on a Linux based Operating System (OS). The Windows version of nginx utilizes the native Win32 API which impacts performance, scalability, and causes other known issues [32]. Installation on Windows Server is therefore not recommended. We use Ubuntu Server 20.04 for the purpose of developing this project. Ubuntu server is a Debian based OS that was created and maintained by Canonical Ltd. Ubuntu server is first installed in either a physical or virtual machine. Nginx is then installed via a single command line. Once installed, reverse proxies are written, and the configuration file is modified. The following commands are executed in a terminal with root access.

```
sudo apt install nginx
```

6.2 TLS Certificates

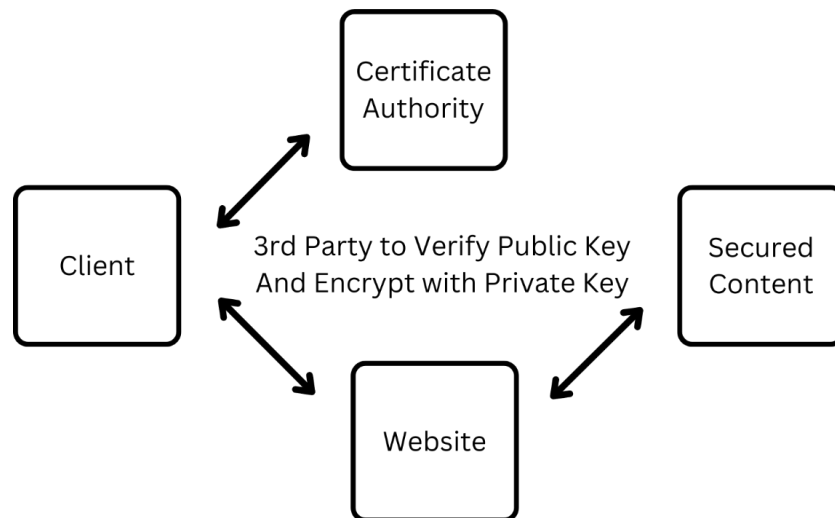


Figure 6.2: Block diagram illustrating the use of TLS Certificates. Securing traffic to a website is performed through a 3rd party Certificate Authority (CA).

Founded in 2014, Let's Encrypt is a free and open-source method of acquiring Transport Layer Security (TLS) certifications. TLS is used for securing connections to a website by encrypting traffic and using a third-party service to authenticate the server. During the initialization of a connection with a server, a handshake exchanges the TLS certificate with the client. A trusted Certificate Authority (CA) is then used to verify the TLS certificate. This is responsible for authenticating Hypertext Transfer Protocol Secure (HTTPS). This is noticeable to users through the presence of the familiar green lock in the browser window. It is important for preventing Man-in-the-Middle (MITM) attacks. MITM attacks occur when a malicious agent attempts to intercept and replace the connection between a client and server. The authentic website is replicated and provided over the connection. This is referred to as a spoof website. This is meant to trick unsuspecting users who will unwittingly provide their credentials or credit

card details. It is otherwise difficult for users to verify the authenticity of a website if it appears to be real. By utilizing a trusted 3rd party, and encryption protocols, we can acknowledge that the server connection is secure.

Certbot is the open-source tool for accessing the TLS certifications offered by Let's Encrypt. It has a Python based plugin for nginx servers which makes signing certifications convenient. The addition of Certbot for writing TLS certificates must be performed after all required networking configurations. The Certbot plugin verifies server accessibility by pulling the certificates from Let's Encrypt. A firewall needs to be installed and the appropriate ports opened. The Uncomplicated Firewall (UFW) is utilized to restrict Local Area Network (LAN) traffic. The primary nginx server will require ports 80 and 443 open for HTTP and HTTPS traffic respectively. Traffic is typically proxied to an available port at the network administrator's discretion. Additional tasks include domain name acquisition, DNS setup, and port forwarding between the primary router and the primary nginx server. The following commands install a UFW and open the required ports. We then proceed to install Certbot for nginx and request a certificate for each domain name. The command line will prompt for an email address to be used for renewal notifications. It will then request to redirect traffic to port 443. Select the second option to confirm redirecting traffic.

```
sudo apt install ufw
```

```
sudo ufw allow 'Nginx Full'
```

```
sudo ufw enable
```

```
sudo apt install certbot python3-certbot-nginx
```

```
sudo certbot --nginx -d yourdomain.com -d www.yourdomain.com
```

6.3 RTMP

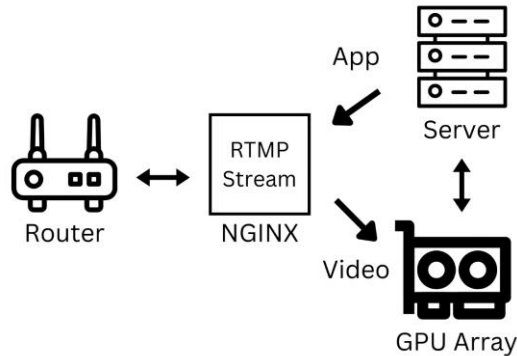


Figure 6.3: Block diagram of an RTMP server. Real-Time Messaging Protocol (RTMP) is used for streaming videos.

Real-Time Messaging Protocol (RTMP) is a protocol used for streaming video content over the internet. It is compact and seamlessly compatible with OpenCV for video processing. Nginx uses a plugin to install and manage RTMP streaming applications. Ports are required to be open on the firewall. It is very important when dealing with video streaming to ensure that only authenticated users can view the stream. All backdoors must be shut to ensure client privacy. The primary nginx proxy is used to restrict stream-reading access to all except a secondary nginx server inside the Local Area Network (LAN). The secondary nginx server is installed on the GPU array with deep learning software. The secondary stream is restricted to viewing on localhost. To facilitate the development of real-time diagnostic services, we create RTMP servers with two streaming paths. One to handle standard color (RGB) video, and another to handle infrared (IR) video. The standard color video may be useful for providing additional information and more precisely aligning facial landmarks on the thermal image. To proceed, we install `libnginx-mod-rtmp` on both primary and secondary nginx servers.

```
sudo apt-get install libnginx-mod-rtmp
```

6.4 Python

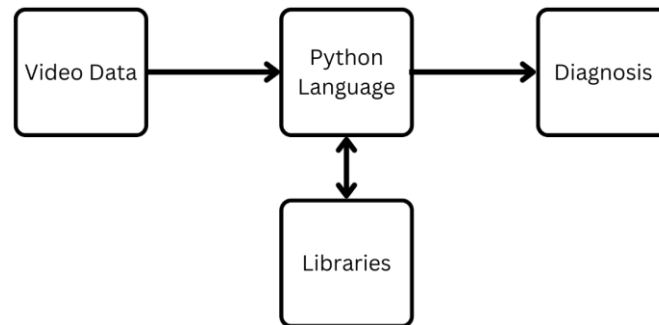


Figure 6.4: Block diagram illustrating the use of Python. The programming language is suitable to read data, access libraries, and perform calculations.

Initially released in February of 1991, Python is a general-purpose programming language which excels at the high-level mathematical computations involved with image processing. It was created to be easy to read and dynamically typed. Python 2 has ceased development, so Python 3 is the recommended version for new projects. Ubuntu server 20.04 ships out with python 3 preinstalled. Python functionality is extended through the installation of packages. To install python packages, the PIP3 utility is required. PIP is an acronym which stands for Preferred Installer Program. In Python, it is used as a recursive acronym which stands for PIP Installs Python. PIP is frequently installed inside virtual environments to avoid interfering with the server OS. This helps provide security at the cost of adding an additional step. It also allows different versions of Python packages to coexist on the same physical machine. This is not beneficial for simple applications or for instances where only one python application is required. The following commands install Python3 and PIP3.

```
sudo apt install python3  
sudo apt install python3-pip
```

6.5 OpenCV

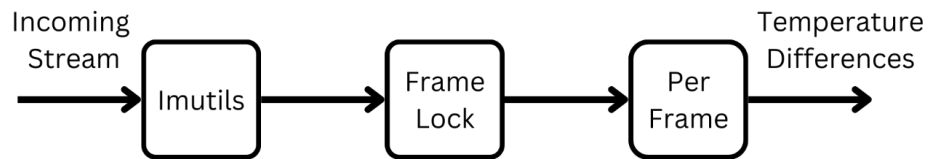


Figure 6.5: Block diagram illustrating the use of OpenCV. Computer Vision libraries manipulate video on a per frame basis.

Initially released in June 2000, OpenCV is an outstanding open-source tool for analyzing video frames. The library contains functions designed for real-time Computer Vision (CV). It is available to run on various platforms, including CPU and GPU based systems. For the fastest processing, GPUs are required. Imutils is a package designed to provide image utilities. Frame locks are used to prevent other aspects of the program from interfering with the frame during analysis. We use OpenCV libraries to annotate video frames with their Augmented Reality diagnosis. Augmented Reality is loosely defined as any system that enhances a user's perception of the real world with computer generated information. While Virtual Reality (VR) aims for the total immersion into a computer-generated world, AR systems attempt to interface with the real world. AR can be realized with a heads up display that allows computer generated numbers or words to be contributed to the field of vision. Contemporary uses of AR include mobile apps that create computer generated animations on live video calls. Our purpose uses live video annotations to provide the real-time diagnosis of respiratory disease. OpenCV can be installed via either PIP or the apt repository.

```
pip3 install opencv-python
```

```
sudo apt install python3-opencv
```

6.6 Flask

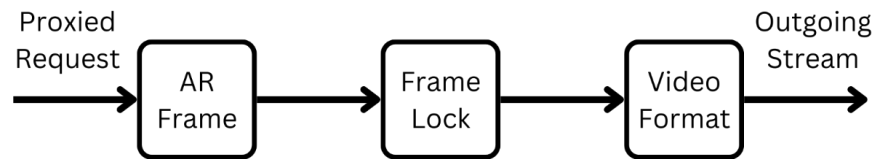


Figure 6.6: Block diagram illustrating the use of Flask. The frame lock must be resolved to process the video stream request.

Initially released in April 2010, Flask is a Python based web server used mainly for developmental purposes. It is very light-weight and fast at rendering web pages in Hypertext Markup Language (HTML). HTML is the language used by websites to render content in a web browser. Flask provides Python libraries which are implemented as code blocks. They are programmed to listen for requests to a specific Uniform Resource Locator (URL). The URL refers to the name of a web resource. A response containing the server resource is generated upon request. For our purpose, Flask works behind the scenes to provide an interface between video processing and webserver software.

Flask facilitates the rapid development of Python applications by unifying the language for video processors and web servers. It is included in many of the popular video streaming demos from GitHub for this reason. The common approach is to acquire a video stream, apply OpenCV to manipulate the video frames, and serve them to localhost for viewing inside a web browser. By utilizing this method, we can implement a variety of algorithms on a live stream and make it accessible for consumption over the web. Flask is installed using PIP via the following command.

```
pip3 install flask
```

6.7 JavaScript

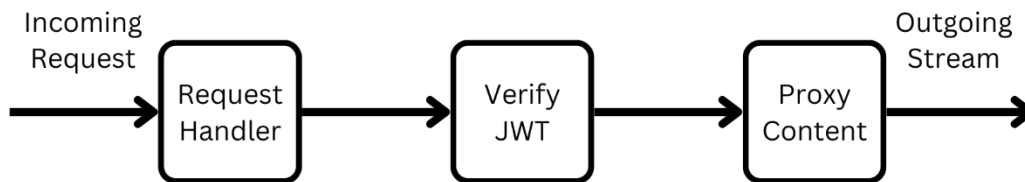


Figure 6.7: Block diagram illustrating the use of JavaScript. JSON Web Tokens (JWTs) are used to authenticate requests for static resources.

For users to set up and configure their video streams, an app must be built to support a User Interface (UI). Android Mobile apps have a file type of Android Package Kit (APK). The Android SDK provides the tools necessary for compiling the program for native installation on Android mobile devices. They can be written in JavaScript or TypeScript. JavaScript is a language which is interpreted at runtime, rather than being compiled. It is designed to operate in a web browser, which makes it ideal for websites. TypeScript is a stricter form of the language which is simply compiled into JavaScript. These programs are wrapped in Cordova and compiled using Android Studio. Cordova is a mobile app platform that provides a web browser environment for native installable apps.

The app must also facilitate user authentication and restrict unauthorized users from accessing content. This is even more imperative for medical applications than your average home-user scenario. The Health Insurance Portability and Accountability Act of 1996 (HIPAA) protects the public against the sharing of personal medical information with anyone other than the patient and authorized representatives. The application allows a user to view the livestream securely by remote login. It uses the principles of token request and authentication to prevent anyone who does not own the account from being capable of requesting resources.

In internet security, there are two approaches. First, protections on the front-end of a website prevent users from mistakenly acquiring inappropriate resources. This is the fastest, easiest approach, but depends on the good nature of users. Malicious users, and potential cybersecurity attacks, will more likely attempt to gain resources from the back-end server directly. This requires a more sophisticated approach to security. NodeJS Express uses middleware authentication for protecting database resources. These are convenient methods which are built into the packages for rapid deployment. Controlling static content is more difficult but relies on the same principles. The server must authenticate the user credentials and determine whether the user can access the material. This is accomplished by verifying the user's identification number matches that of the static content or video stream channel. The identification number is stored with the static resource.

The difficulty lies in the speed at which static content is usually requested. Websites with lots of images generate numerous server requests with each page turn. Quick authentication methods are required to reduce delays. JSON Web Tokens (JWTs) are commonly used for online app authentication protocols. They are fast, lightweight, and highly secure. They are decoded using a secret on the server, to check for malformations that indicate foul play. The problem with web tokens is that anyone who has the token can access the associated user resources until the token has expired. Token expirations are usually no more frequent than 24 hours. Otherwise, the users are required to log-in an excessive number of times. It is therefore important to hide the JWT during server-client communications, so that bad actors cannot acquire user credentials by monitoring network activity. To secure static content, a secondary JWT is obtained by client request to the server. The standard app JWT is hidden in the real-time request and authenticated via the middleware.

6.8 Video Streaming

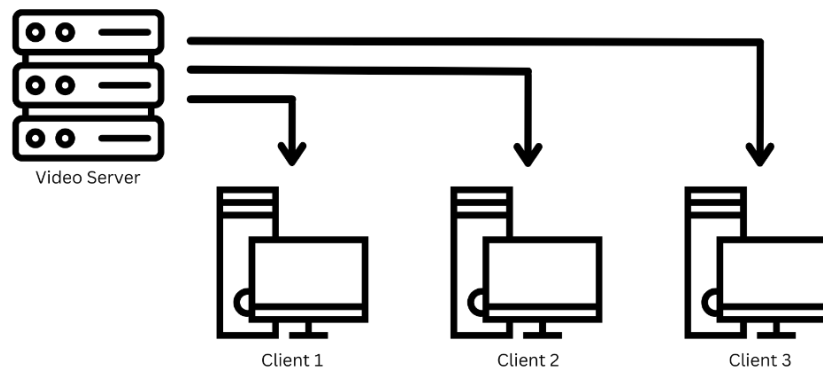


Figure 6.8: Illustration of unicast streaming. The video stream is sent from the server to each client over separate connections.

Unicast streaming is chosen over multicast streaming for its simplicity and security. In unicast streaming, each client-server connection receives its own media stream. Multicast streaming shares the stream among multiple clients, which saves server bandwidth. MJPEG-streamer is frequently used for software development demonstrations involving video streams. This is due largely to the ease and effectiveness of configuration. It involves sending a stream of video frames that are individually encoded in JPEG format. These are displayed consecutively inside an HTML image tag, ``. Within an image tag, the source property is set to the video stream URL address. The width property is set to restrict the display size of each video frame, without interfering with the aspect ratio. The alternative text property is set to display a text-based representation of the image, which can be viewed with a mouse hover over the image, or when accessed with a screen reader. The alternative text property is frequently overlooked by web developers. The Americans with Disabilities Act of 1990 (ADA) provide requirements to ensure web accessibility for the impaired. Screen readers use the title and alt text attributes of an HTML image tag to provide an audio-based representation. This ensures a website does not discriminate against the visually impaired.

In ideal circumstances, MJPEG streaming provides the highest quality video with the least amount of code. Unfortunately, it also consumes vast quantities of bandwidth. This makes it difficult to view MJPEG streams over mobile devices or within busy networks. Performance varies dramatically based on network conditions and device capabilities. Additionally, continuous streams of data are discouraged by developers. Packages are sent over the internet in bursts, to facilitate asynchronous operation. Bursts are designed to send the maximum amount of information able to be transmitted over a connection. Since this is an unknown variable, servers begin transmitting in short bursts. Transmission bursts lengthen until the client reports missing data. At this point, the transmission resumes with shorter burst lengths.

This problem can be solved by saving video frames into volatile memory. The frames are compiled into short video segments. Efficient video formats require less bandwidth to transmit than individual frames. This is because video formats track pixel changes between frames, rather than sending each frame individually. There are numerous video formats to choose from, but MP4, WebM, and Ogg are recommended due to their compatibility with HTML. The <video> tag is used to display videos on webpages. It has similar attributes as the tag, but with the addition of user controls for manipulating playback. The videos can be played automatically by including the autoplay property. Each video segment can be 1 second or less, to reduce lag time. Lag time will result from the combination of transmission, processing, and video saving processes. With the proper adjustment of frame rate and segment length, an appropriate balance between bandwidth and lag can be achieved. It is important to minimize lag time for AR applications. If the image does not appear in real-time, the sensation of augmented reality will be lost on a user.

6.9 Summary

Enterprise streaming software is the missing link between medical IRT and the real world. To effectively process video, more powerful GPU hardware can be deployed. Streaming over the internet can allow mobile users to access this power-hungry GPU architecture. Nginx is a popular software tool for securing apps through reverse proxy and handling TLS certifications. It is also capable of being modified for RTMP video streams. We deploy nginx for these reasons as a primary reverse proxy to handle video streams. Python, OpenCV, and Flask are utilized for the image processing and restreaming aspects of this project. By taking a video stream apart in real-time, annotating each frame with calculated data, and restreaming it to the client, medical diagnosis and vital signs measurements can be viewed by the client. This software stack provides the foundation for AR based systems.

JavaScript is an essential aspect of web-based technology. It is used by this project to provide user interfaces and authentication protocols. JWTs are issued to secure user accounts and prevent unauthorized access to static web content. This twofold approach prevents malicious users from attacking a webserver from either the front door or the back door. Finally, we discussed video streaming and made note of the issue created by MJPEG streaming. It consumes too much bandwidth for smooth operation on mobile devices. The solution of saving frames into memory to be encoded into short videos is mentioned as the obvious next step.

Chapter 7: Computer Vision

Facial Recognition software has a long history as one of the first widely used applications of image processing. Deep Learning (DL) software is the new standard for performing facial recognition on RGB images. We proceed with a commonly used Dlib prediction model for annotating facial landmark locations on standard images. The typical models don't work on thermal images due to a lack of contour details, resolution, and training data. The inclusion of a homography matrix is discussed to translate ROI coordinates from RGB to IR images. This still requires a method of accurately tracking a few corresponding datapoints on the thermal image. Machine Learning (ML) and Deep Learning (DL) versions of a prediction model that have been trained with thermal images are used to provide accurate facial landmark annotation for IRT.

Color spaces are introduced because of the pseudo color palettes associated with thermal imaging systems. We consider the difference between additive and subtractive color spaces. The Euclidean distance is commonly used to find the difference between two colors in a space. Because thermal cameras measure a narrow band of frequencies, we use the grayscale to estimate the difference of pixel intensities. A Gaussian blur function reduces the effect of noise on temperature measurements. Noise reduction is further improved by averaging the intensity of all pixels within a select ROI. The difference of pixel intensities will depend on automated calibration and temperature scaling. This will be subject to the type of thermal camera and various environmental factors. Temperature references are suggested to reconcile the difference in pixel intensities that could result from automatic temperature ranging. The temperature color scale should ideally be used as a reference.

7.1 History of Facial Recognition



Figure 7.1: Block diagram of facial recognition. Note the process happens on a per frame basis. Modified from [6].

Daniel et al provide a brief history of face recognition technology [6]. One of the most challenging aspects of image-based facial recognition is the number of variables that arise in real-life circumstances. Lighting, camera angle, distance, resolution, obstructions, age, demeanor and other environmental variations can change how a face appears in a 2-dimensional image [6]. Early demonstrations indicated that computer algorithms were able to identify faces under controlled conditions [6]. In the early 70s, a more geometric-based approach using contours and edges were proposed by Kelly's and Kanade's PhD theses to identify faces via the Procrustes distance between facial landmarks [6]. While geometric-based algorithms were not as accurate as the holistic methods, it was faster and required less memory [6].

Holistic methods utilized more information by analyzing the whole face [6]. A common approach was to use Principal Component Analysis (PCA) to create a space of eigenvectors that illustrate the variance between training images [6]. The eigenvalues create face-like images and were called eigenfaces [6]. "New faces can be projected onto the subspace spanned by the eigenfaces to obtain the weights of the linear combination of eigenfaces needed to reconstruct them" [6]. The projection of eigenvectors onto the eigenface subspace yields an error vector that is normal to the subspace. The eigenvector with the minimum error is a likely match.

Deep Learning (DL) with Convolutional Neural Networks (CNNs) provide more capable facial recognition algorithms [6]. They rely on large datasets to automatically learn the variations of features within the training data [6]. This allows DL facial recognition to identify faces with new variations, as long as they can be generalized from previous examples [6]. The time and cost of labeling large datasets for training purposes is a limiting factor of DL methods. A few databases have been made available to the general public for this reason. In order to facilitate the acquisition of larger datasets, new images can be created by manipulating facial expressions, applying aging algorithms, mirror imaging, adjusting the brightness or contrast, and other computer-generated methods [6].

Kong et al discuss the recent advances in facial recognition for both visual and infrared spectrums. The facial recognition problem is difficult because of the changes in lighting, background, and facial features [25]. Continuing research into facial recognition is focused on identifying faces in the infrared spectrum. Infrared facial recognition is beneficial because IR light is mainly emitted, not reflected. Therefore, less variability exists between environments with different lighting [25]. There are numerous applications of infrared face detection. Facial recognition and expression interpretation are vital aspects of smart environments [25]. The ability to identify faces and facial expressions in the dark is highly desirable. While driving at night, the interiors of automobiles are kept dark to facilitate visibility of the road. Drowsiness detectors need to function in limited and no light conditions to alert drivers who are experiencing fatigue. Security systems depend on their ability to function when all other power and lighting systems have failed. Thermal cameras are required to identify intruders in the dark. Facial biometric data need to function regardless of lighting conditions. Finally, wildlife detectors should be able to tell the difference between humans and animals at night.

7.2 RGB Facial Landmarks

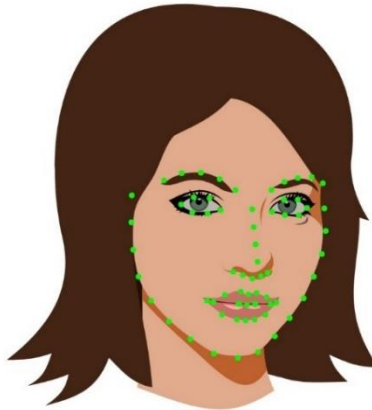


Figure 7.2: Example of facial landmark annotation on a standard model. The 68-point shape predictor is deployed by Dlib.

Dlib-ml is an open-source library designed for cross platform implementation of machine learning into C++ applications [23]. It uses Basic Linear Algebra Subroutines (BLAS) to programmatically find the optimal solutions to equations that are written in a form like MATLAB [23]. Linear Algebra is the mathematical framework that encompasses vector and matrix operations [40]. The modular design allows parameterized algorithms to be independent from the data type [23]. The Dlib shape predictor model is used to determine select data points, called landmarks, on a human face. The library is run on standard color images to identify regions of the face for analysis. Thermal images typically display less resolution and fewer defining features than standard color images. Combined with the lack of thermal images to use as training data, it becomes difficult to create face detection models for thermal images. The FLIR system has both infrared and standard color photosensors.

```
detector = dlib.get_frontal_face_detector()
predictor = dlib.shape_predictor('path_to_model')
```

7.3 Homography Matrix

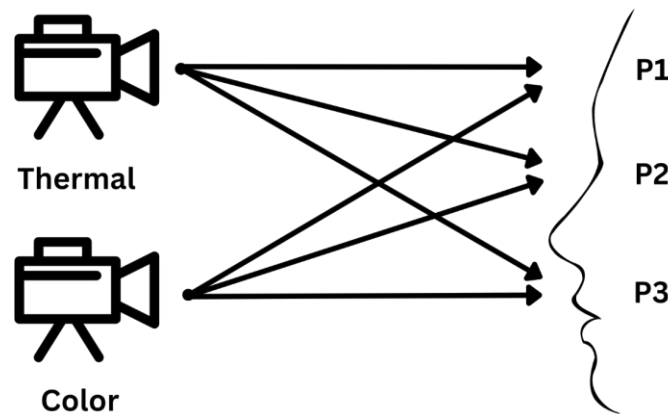


Figure 7.3: Diagram of two cameras recording a human face. This illustrates the use of a homography matrix in video processing.

Baskaran et al proceed to evaluate various deep learning algorithms that can be used to detect facial landmarks on thermal images [2]. DL algorithms have been successfully tested for labeling emotions and determining sobriety [2]. They note that there already exist facial landmark detection algorithms which are highly accurate for standard color photos [2]. Attempting to convert thermal images to standard color images did not produce reliable results for facial landmark detection [2]. Instead, a homography matrix is utilized to achieve facial landmark detection on thermal images. A homography matrix maps the location of each ROI between two images taken at the same time using different cameras. It is used in computer vision to relate any two images of the same planar surface. Homography matrices can be employed to track motion, render navigation, and place 3D models into videos. It assumes the pinhole camera model, which is a close approximation to standard RGB color cameras. The focal plane arrays of modern thermal cameras are slightly larger than pinholes; but the approximation should still be valid.

Existing face detector models will not work reliably on low resolution thermal images. There is not enough resolution or information to clearly define the contours of the face. Since the FLIR ONE Pro system has both visible and infrared cameras, we can take images in both spectrums. This allows for standard face detection algorithms to be run on a standard image. Once identified, coordinates for the regions of space to be analyzed are translated to the corresponding thermal image.

Video processing requires a method of tracking ROIs in both standard and infrared spectrums. Dowdall et al examine the typical tracking algorithms and find they are not effective at tracking objects from infrared videos [8]. They propose a novel face tracking method based on coalitional game theory. Because individual trackers are not dependable, they distribute the tracking functionality across a network of trackers that operate in coherence. The relationship is modeled after coalitional game theory. The trackers form players, and the teams consist of their coalition. The winning team of trackers is used for calculating the position of the object [8]. By considering the influence of neighboring trackers, overall performance is increased. It functions adequately on both infrared and standard video.

For AR realization, the program uses multispectral data. Both RGB and IR videos are streamed to the backend. OpenCV analyzes the temperature differentials measured in the infrared spectrum of data. The program then provides the user with a diagnosis written on the video stream taken using the visible light spectrum. This provides users the allusion of being diagnosed from a regular video. The standard image also serves the purpose of identifying regions of the face to be analyzed and creating the homography matrix. Novice users do not need to be aware of the multispectral nature of the sensor. Experienced users could switch between AR and IR modes of operation.

7.4 IRT Facial Landmarks

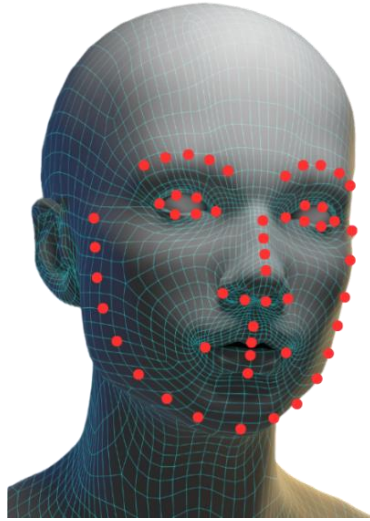


Figure 7.4: Example of facial landmark annotation on a thermal model. Landmarks are manually annotated on a mask to reflect anatomical locations more clearly.

Kuzdeuov et al created two facial landmark detection algorithms for thermal images using ML and DL models [27]. They note the importance of facial landmark detection for computer vision applications [27]. There are numerous datasets of images taken in the visible spectrum, but relatively few in the infrared spectrum [27]. Kuzdeuov et al present a new dataset, SF-TL54, based on their previous work recording Speaking Faces with thermal and visible cameras [27]. The Speaking Faces dataset recorded 142 participants from 9 different angles while subjects read passages from a prompt. Images taken in the visible spectrum were analyzed with Dlib facial landmark prediction [27]. The FLIR T540 thermal camera, with 464x348 pixel resolution, was used to record the thermal data [27]. This provided large amounts of data, which was later augmented via photo editing. It is a common practice to augment image datasets for facial recognition. By mirroring each image, the dataset can be doubled with a keystroke. This is possible due to the symmetrical nature of human faces and vast capability of photo editing software.

The facial landmarks did not line up with corresponding thermal images, because they were taken with two different cameras [27]. A homography matrix would be required to translate the coordinates of facial landmarks between images. This still requires some form of object detection in the IR spectrum. Instead, the thermal images were manually annotated with the locations of facial landmarks with the help of photo editing magic. Thermal images were converted to grayscale, inverted to obtain the negative images, and gamma corrected to enhance brightness [27]. This process served to increase the contrast of thermal images to make them visually identifiable. Despite visual cues, the thermal images still required manual annotation for training purposes. Kuzdeuov et al used their dataset to create two different algorithms. An ML model via Dlib shape predictor and a DL model based on U-net architecture both demonstrated satisfactory accuracy [27].

A comparison of the libraries demonstrates when they are most effective. The Dlib shape predictor runs faster and is better suited to running on a Central Processing Unit (CPU) [27]. The ability to run on CPUs makes the ML approach more appealing to run on embedded Linux platforms like the Raspberry Pi. Testing demonstrates the ML library functions adequately on a Raspberry Pi 4 model B. The DL model is more accurate but runs slower [27]. The DL model is better suited to run on a Graphical Processing Unit (GPU). The performance of GPUs and CPUs will depend on the type of operation. CPUs handle simple calculations at blistering speeds. GPUs handle more specialized tasks with mathematical algorithms designed for computer graphics. GPUs typically require more hardware and power to operate. They are not considered portable for this reason. Video streaming protocols are utilized to transport videos from a portable camera to the GPU infrastructure. In this way, DL algorithms can be applied to thermal images in real time.

7.5 Color Space

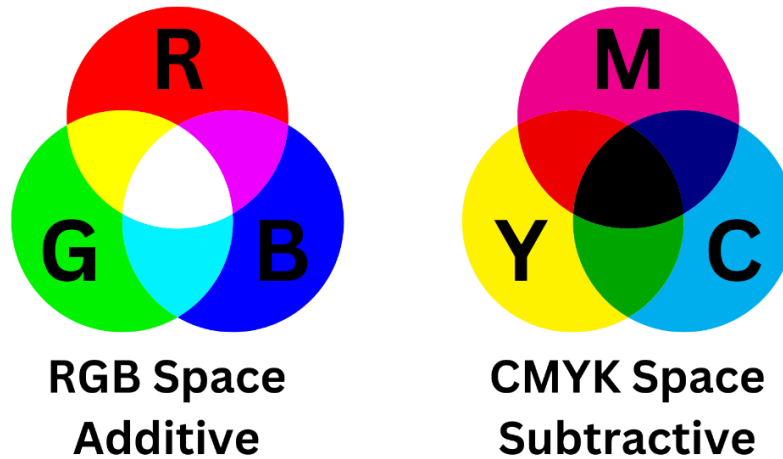


Figure 7.5: Illustration of additive and subtractive color spaces.

Color space is the organization of colors into combinations of color models and mapping functions available for an application. It defines the specific range of achievable colors and pixel intensities. A color model represents colors in numerical arrays, called tuples. The mapping function defines a new color space by correlating it to a referenced color space. It can be applied to computer programming and related to human vision. The Red Green Blue (RGB) color model used to display images on computer screens is additive. Combining RGB pixels emitting light at equal intensity creates the color white. This is because the radiation of EM energy is additive. On the other hand, the Cyan Magenta Yellow and Black (CMYK) color model used to print images on paper is subtractive. Combining the colors in a splotch of paper creates the color black. This is because the reflection of EM energy is subtractive. The ink is colored because it reflects that frequency of light but absorbs other wavelengths from the spectrum. We can only see colors that have been emitted or reflected from an object. When RGB spectrums of light reach the retina, humans see the color white. Black is merely the absence of light.

7.6 Euclidean Distance

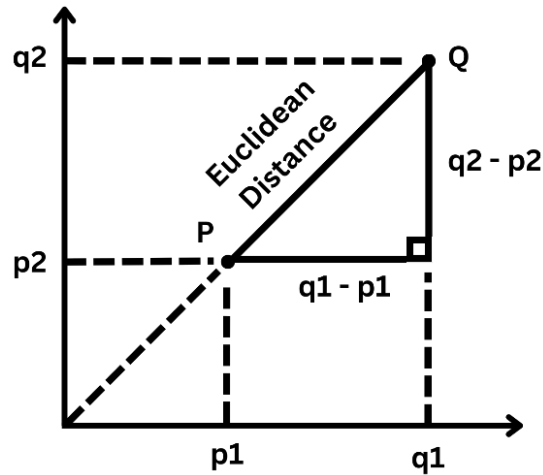


Figure 7.6: Diagram of the Euclidean distance in two dimensions. Used for calculating the difference between two colors in a space.

The difference between two colors is estimated by the Euclidean distance between two points, p and q in three dimensions. The points are compared by squaring the difference of relating RGB pixel values. The square root is calculated from the addition of squared differences. Here, the numerical subscripts r , g , and b represent the pixels RGB respectively.

$$d(p, q) = \sqrt{(p_r - q_r)^2 + (p_g - q_g)^2 + (p_b - q_b)^2}$$

In thermal imaging, pseudo colors are used to represent temperatures. Automatic temperature calibration allows the thermal images to be visually useful in a wide range of environmental conditions. To preserve accuracy, a scale is usually provided which maps the values of temperature with their associated color space. The temperature corresponds to the RGB pixels with the least Euclidean distance on the scale. This enables visual and computational indication of temperature distribution across a thermal image.

7.7 Grayscale

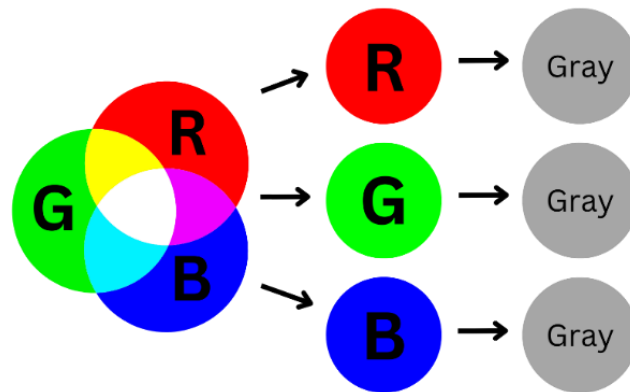


Figure 7.7: Illustration of RGB image decomposition into grayscale. The image is separated into RGB components and converted into their respective grayscales.

The grayscale is a color space that does not contain color. Instead, it consists of white, black, and the shades of gray in between. Grayscale images are created by measuring the intensity of light at each pixel. It is most accurate when only one frequency of light is considered. This is the primary basis for IR camera displays and what the thermal camera sensor is actually recording. Thermal cameras record a relatively narrow frequency band. Pseudo color palettes are created on top of the grayscale image. When converting an image from RGB to grayscale, the average intensity of each RGB value is applied to all RGB values. Formulas can be used to weight the RGB pixel components and create various artistic effects. Weights are constants such as x , y , and z that multiply the RGB pixel components. The following function demonstrates weighted RGB to grayscale conversion. Unweighted RGB to grayscale conversion is achieved by setting the weighted constants equal to one.

$$gray(R, G, B) = \frac{(x \cdot R + y \cdot G + z \cdot B)}{3}$$

The use of a single point for temperature measurement is problematic. Errant pixels due to noise can change results at random. It becomes a very noticeable issue with image processing. The beauty of modern thermal camera systems is their automatic noise reduction and temperature scale calibration. The raw image details only provide the grayscale intensity differences. Programs that were created using a thermal camera's official API can acquire the temperature color scale for reference. This should be included whenever possible to acquire absolute temperature measurements. The inclusion of temperature scale information does not by itself provide a diagnosis. For our purposes, we are mainly interested in the relative temperature measurements obtained by averaging the difference of pixel intensities between various ROIs.

A gaussian blur function reduces noise by averaging the pixel intensity between neighbors. This is less susceptible to noise when taking temperature values based on single pixels. The approach of averaging can be taken a step further by finding the mean value of all the pixel intensities within a given ROI. If the temperature scale is accessible by the application, these color values can be compared to extract an average focal temperature value. If the temperature scale is not accessible, the application is restricted to measuring the difference of intensities. The problem with color differences, is that different cameras under different environments may exhibit different pseudo color palettes and therefore require different thresholds to achieve the same diagnosis. Regardless, the average pixel intensity within an ROI is less susceptible to noise than per pixel calculations. The size, shape, and position of the regions are determined by performing vector analysis on facial landmark coordinates. This ensures the approach is viable regardless of exact distance from the camera, and size of the patient. By using existing face detection models, and simple math, we subvert the largest issues facing current scientific works.

7.8 Results

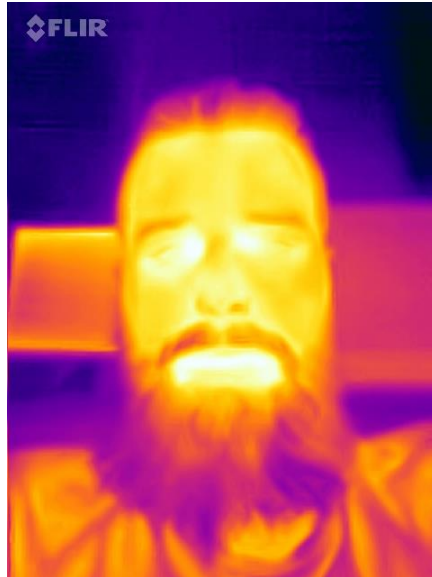


Figure 7.8: Thermal image of a healthy face. Demonstrates normal temperature distribution. Taken by a FLIR ONE Pro.



Figure 7.9: Thermal image of a URTI infected face. Demonstrates inflammation of the nasolacrimal ducts. Taken by a FLIR ONE Pro.



Figure 7.10: RGB image of oral cavity. Demonstrates inflammation of the throat during a URTI. Taken with an Android mobile device.



Figure 7.11: Image of antigen test for Covid-19. Demonstrates the URTI was not caused by Covid-19. Taken with an Android mobile device.

Author was experiencing symptoms of a sore throat, runny nose, and fatigue. A visible image of throat demonstrates oral lesions. A thermal image of the face demonstrates fever, inflammation of the lacrimal caruncles, and inflammation of the nasolacrimal ducts. It should represent a common URTI. Over The Counter (OTC) antigen test for Covid-19 yielded a negative result. The nasolacrimal duct system drains into the nasal cavities and throat. In most cases, sneezing is an earlier warning sign than coughing. The throat was already inflamed therefore the patient was symptomatic. The pre-symptomatic case would expect to find reduced temperature on the center forehead, before a fever begins.

7.9 Summary

We began with a history of facial recognition. ML and DL algorithms are now commonly used for face detection in industry. They are frequently applied to biometric identification, emotion reading, and attention tracking. We learned about automated facial landmark annotations for standard RGB images. A method to translate landmark datapoints from an RGB image to a thermal image was discussed. The coordinate points and sizing for all ROIs must be translated from the standard RGB image into the thermal image. For real-time calculations, two video streams would be required. This requires additional bandwidth and computer power to process the additional video stream. Fortunately, facial landmark detection has been successfully demonstrated for thermal images. We discussed how the dataset was created and that the ML model would be better suited for running on embedded Linux devices like the Raspberry Pi.

Color space was discussed because of the pseudo color palettes associated with thermal images. The difference of colors was considered as the Euclidean distance between two points in a three-dimensional color space. These methods represent developmental dead-ends. They will not yield reliable interpretations of thermal images. Thermal cameras sense the intensity of IR light on pixels within a focal plane. The detection is limited to a narrow band of frequencies. By using the grayscale, we are observing the closest version of what a thermal camera is able to record. Single pixel values are susceptible to noise. Gaussian blurs and the averaging of pixel intensity across ROIs provide more stable results.

Chapter 8: Conclusions

Medical IRT is a rapidly developing field. It has been demonstrated useful in detecting numerous different pathological conditions. It has also been demonstrated to be inconsistent and misleading. IRT hasn't been adopted by the medical community, due to the difficulty interpreting results and the cost of calibrating sensors. Ironically, medical IRT was only hailed as a promising new technology, until IR cameras were made readily available to consumers.

ML and DL algorithms to detect facial landmarks exist for both visual and thermal images. ROIs are calculated by performing vector analysis on the coordinates of known facial landmarks. Color differences between the ROIs are used to infer the presence or absence of pathological conditions. The difference between two colors is calculated by finding the Euclidean distance between two points in three dimensions. The RGB color space is commonly used for displaying images on a computer screen, but grayscale is a better representation of thermal images.

Dynamic measurements such as HR and RR can increase the accuracy of a remote diagnosis. Core and peripheral body temperatures can be elevated by fever, stress, and environmental conditions. Nasolacrimal inflammation can be caused by URTIs, allergies, and obstructions. We propose that it is unlikely to find both fever and nasolacrimal inflammation in patients that are not actively fighting a URTI. By combining the evaluation of core body temperature, peripheral body temperature, and vital signs measurements with inflammation of the nasolacrimal duct, we create a more reliable method of remotely diagnosing respiratory illness.

8.1 Discussion

Diet, exercise, stress, time of day, biological cycles, and other factors can influence thermoregulation in humans. This is why related works combine HR and RR with core body temperature. The combination of vital signs provides a better indicator of disease than any one variable. It is also more robust against the differences in sensitivity between various thermal cameras. But elevated vital signs do not exclude the possibility that a patient was just running to catch a flight or otherwise experiencing anxiety. Finding an additional marker is essential for creating an accurate remote diagnostic tool. The nasolacrimal duct is evaluated for such purposes due to its proximity with common vectors of infection. We compare the core temperature, peripheral temperature, HR, and RR, with the nasolacrimal duct temperature to make an improved algorithm for remote diagnosis. Inflammation of the nasolacrimal ducts is not exclusive to cold and flu symptoms. Allergies and other forms of irritation can also cause inflammation. But the causes of nasolacrimal duct inflammation are unlikely to coincide with increased vital signs.

Facial landmarks are used for identifying and tracking the regions of interest. This technique can be applied to both visual and thermal spectrums. Homography matrixes are used to translate coordinates between images. This enables the sophisticated object detection that was developed for visual images to be applied to thermal images. Color differences can serve as viable indicators. The absolute temperature is not required, only the relative difference of temperature between ROIs. We can't measure absolute core body temperature readings with the current configuration because the color scale information is not available. The color differences are compared between core and peripheral regions of interest (ROIs). This is a more reliable approach than absolute temperature readings.

8.2 Limitations

The app is limited by several factors. Infrared sensor resolution will restrict the distance from the patient that accurate measurements can be taken. We do not currently know the distances at which measurements are valid. The standards for IRT in fever detection illustrate that the average intensity of at least 9 pixels is required to accurately measure the temperature of each lacrimal caruncle. This provides a foundation for maximum camera distance based on sensor resolution. Further limitations may include exogenic sources of infrared radiation, such as sunlight or heat lamps. Proper precautions should be taken to reduce thermal noise. Inclement weather is expected to affect the temperature measurement of peripheral extremities. The patient should be allowed to relax and their body to reach thermal equilibrium with the ambient room temperature. Another limiting factor may include endogenic sources of infrared radiation, such as excess body heat from fever or exercise. This provides another reason to allow the patient to rest and reach thermal equilibrium with their environment and homeostasis. While color intensity differentials are chosen to mitigate these factors, more study will be required to know if these limiting factors can be overcome in the future.

We can't extract absolute temperature measurements without obtaining the color scale information. Thermal images can be presented in a range of pseudo color palettes used to visualize temperature patterns [35]. A common feature among thermal cameras is the range of pseudo color palettes available from which to select. They use a color scale to associate the pseudo color palette with measured temperature [35]. The color scale and palette information should be included in study results to provide the most information possible [35]. This information will need to be obtained from the sensor and interpreted by the application. This will enable absolute temperature measurements, from a select group of compatible sensors.

8.3 Applications

Kiosk based devices hold the most promise for applications regarding public deployment. Entranceways to public places could use this technology to limit the spread of contagious respiratory illness. This would mitigate the threat of future global pandemics such as Covid-19. Airport screenings could be quick and accurate enough to safely board passengers between flights. Schools and universities can limit the number of sick students and missed classes. Hospitals can use it for triaging patients that enter the emergency room. Patients can be quickly triaged into separate departments that are designed to handle each case. Minute clinics could use it to quarantine contagious patients in the waiting area. Patients that screen positive for contagious respiratory illnesses could be contained in specialized waiting rooms that are hermetically designed for pathogenic isolation. This would protect doctors and patients by limiting transmission of contagious respiratory infections.

Mobile phone-based devices hold the most promise for applications regarding private use. This is because numerous individuals already own a mobile phone. Only the addition of a thermal camera attachment and internet access is required. The careful deployment of medical IRT onto a mobile app can be used to teach the public about science and medicine. By providing a low-cost solution, we reduce the barrier to education and learning. Education is the primary mechanism to alleviate fear of the unknown. It is their fear that ultimately drives patients to purchase the diagnostic services from a physician. The goal is to reduce pressure on doctors and emergency rooms, by limiting the frequency of visitation due to simple URTIs. Biometrically verified scan results could be displayed from the secure mobile app to avoid the requirement of being scanned by public utilities as mentioned above. This is important for individuals who may be concerned about privacy.

8.4 Further Development

The app can be taken a step further by addressing some of the currently known limitations. Additional diagnosis can be included to provide more functionality from the same application. For example, the kiosk can be further developed to include an RGB camera. This will provide multispectral data which can be compared with a homography matrix. This facilitates additional features, such as standard object detection and face recognition algorithms. Once an object or feature is recognized in the visual spectrum, temperature analysis can be performed on the IR spectrum. Breast cancer detection could be included after training deep learning models to detect thermal breast images. This would trigger a different function in the program to search for hot spots and analyze temperature differentials in the breast tissues. To interpret thermal images of distal forearm fractures, models would be trained to identify the pair forearms. Temperature differentials could be used to indicate percentage gained in the healing process. More diseases can certainly be identified and trained appropriately. But the applications of multispectral imaging do not end with medicine. Facial recognition can be used to verify the identity of the individual that is being scanned. This would limit the need for authorities to view a person's identity. External switches can be added for controlling a gate mechanism. This can be used to prevent contagious individuals from accessing tightly controlled spaces. The IR sensor should be further developed for increased resolution and framerate. The temperature range and pseudo color palette information should be obtained from the sensor and provided to the webapp. This will facilitate the inclusion of absolute temperature measurements. The TOPDON TCView TC001 thermal camera is not currently available for iPhone mobile devices. An additional sensor module with iPhone compatible USB port is required. IOS compatible mobile apps are also necessary to take advantage of this user base.

8.5 Final Thoughts

The fundamental aspects of kiosk and mobile apps were built and demonstrated to be functional. Images taken of the author confirms the inflammation of the nasolacrimal duct during a respiratory illness and demonstrates its usefulness in medical diagnosis. Limitations include viewing angles, pixel resolution, and distance from the camera. Applications include stopping the spread of contagious illness, enhancing the speed and accuracy of medical triage, and reducing the reliance of people on doctors. Further developments will refine the current mobile app and generate multiple algorithms for more diagnosis.

With numerous applications to consider, the importance of medical IRT cannot be overstated. It is equally important to accurately record and interpret IRT data. Misdiagnosis of medical IRT images can result in untreated diseases, unwarranted medical procedures, and the ultimate dismissal of a valuable tool. In the 1970's, early infrared imagers were constructed with scanning elements and kept cool with liquid nitrogen [38]. These primitive scanning devices were sensitive to variations in coolant levels [38]. It is now known that this could have been a factor in the early dismissal of IRT by the medical community. The average thermal cameras at the time could measure a temperature difference of 0.5 degrees Celsius, at a rate of 1-16 FPS, and limited resolution [35]. These devices were expensive, bulky, and ineffective.

Modern IR cameras are now relatively inexpensive, with high fidelity. But the greatest advancements in the field of IRT has been with software. New digital imaging and CV techniques have reopened the possibilities for medical IRT. Facial landmark annotation for thermal and standard images makes it possible to accurately calculate ROIs in either spectrum. The standardization of HTTPS and video streaming protocols facilitate the use of more powerful server infrastructure.

References

- [1] Abdulhamid, Mohanad, Otieno Odondi, and Muaayed Al-Rawi. "Computer Vision Based on Raspberry Pi System." *Applied Computer Science (Lublin)* 16.4 (2020): 85–102. Web.
- [2] Baskaran, Ruben et al. "Using Facial Landmark Detection on Thermal Images as a Novel Prognostic Tool for Emergency Departments." *Frontiers in artificial intelligence* 5 (2022): 815333–815333. Web.
- [3] Bouzida, Nabila, Abdelhakim Bendada, and Xavier P. Maldague. "Visualization of Body Thermoregulation by Infrared Imaging." *Journal of thermal biology* 34.3 (2009): 120–126. Web.
- [4] Byrnes, J. S. *Unexploded Ordnance Detection and Mitigation*. Ed. J. S. Byrnes. 1st ed. 2009. Dordrecht, Netherlands: Springer, 2009. Web.
- [5] Ćurković, S et al. "Medical Thermography (digital Infrared Thermal Imaging – DITI) in Paediatric Forearm Fractures – A Pilot Study." *Injury* 46 (2015): S36–S39. Web.
- [6] Daniel Sáez Trigueros, Meng Li, and Margaret Hartnett. "Face Recognition: From Traditional to Deep Learning Methods." *arXiv.org* (2018): n. pag. Web.
- [7] Dhatt, Saroop, and Paul Winston. "The Role of FLIR ONE Thermography in Complex Regional Pain Syndrome: A Case Series." *American journal of physical medicine & rehabilitation* 100.4 (2020): e48–e51. Web.
- [8] Dowdall, Jonathan, Ioannis T. Pavlidis, and Panagiotis Tsiamyrtzis. "Coalitional tracking in facial infrared imaging and beyond." *2006 Conference on Computer Vision and Pattern Recognition Workshop (CVPRW'06)*. IEEE, 2006.
- [9] Eccles R. Understanding the symptoms of the common cold and influenza. *Lancet Infect Dis.* 2005 Nov;5(11):718-25. doi: 10.1016/S1473-3099(05)70270-X. PMID: 16253889; PMCID: PMC7185637.
- [10] Fei, Jin, and Ioannis Pavlidis. "Thermistor at a Distance: Unobtrusive Measurement of Breathing." *IEEE transactions on biomedical engineering* 57.4 (2010): 988–998. Web.

- [11] "File:Black body.svg." *Wikimedia Commons, the free media repository*. 31 Jul 2022, 04:25 UTC. 17 Feb 2023, 16:47
<https://commons.wikimedia.org/w/index.php?title=File:Black_body.svg&oldid=679200869>.
- [12] "File:Gray1199.png." *Wikimedia Commons, the free media repository*. 20 Apr 2021, 05:19 UTC. 16 Feb 2023, 20:17
<<https://commons.wikimedia.org/w/index.php?title=File:Gray1199.png&oldid=554067204>>.
- [13] "File:Gray896.png." *Wikimedia Commons, the free media repository*. 20 Apr 2021, 05:14 UTC. 16 Feb 2023, 20:03
<<https://commons.wikimedia.org/w/index.php?title=File:Gray896.png&oldid=554066124>>.
- [14] "FLIR Launches Five New Thermal Cameras: Third Generation FLIR ONEs, FLIR Duo Thermal/Visible Drone Cameras, and FLIR C3 Rugged Pro Camera." *Measurement and control (London)* 50.2 (2017): 22–23. Web.
- [15] "FLIR ONE Pro Thermal Camera." Edited by Sara Scullin. *Professional Tool & Equipment News* 30.1 (2019): 46–46. Print.
- [16] Fraser, Jennifer. "Hot Bodies; Cold War: The Forgotten History of Breast Thermography." *Canadian Medical Association journal (CMAJ)* 189.15 (2017): E573–E575. Web.
- [17] Garbey, Marc et al. "Contact-Free Measurement of Cardiac Pulse Based on the Analysis of Thermal Imagery." *IEEE transactions on biomedical engineering* 54.8 (2007): 1418–1426. Web.
- [18] Grozdanova-Uzunova, R. "Infrared Thermography in the Diagnostics of Hidden Infections – Case Reports." *Journal of Physics. Conference Series*. Vol. 1859. Bristol: IOP Publishing, 2021. 12040–. Web.
- [19] Hollenberg, Alex M et al. "Electromagnetic Stimulation Increases Mitochondrial Function in Osteogenic Cells and Promotes Bone Fracture Repair." *Scientific reports* 11.1 (2021): 19114–19114. Web.
- [20] Hosny, Khalid M et al. "COVID-19 Diagnosis from CT Scans and Chest X-Ray Images Using Low-Cost Raspberry Pi." *PloS one* 16.5 (2021): e0250688–e0250688. Web.
- [21] Jaspers, M.E.H. et al. "The FLIR ONE Thermal Imager for the Assessment of Burn Wounds: Reliability and Validity Study." *Burns* 43.7 (2017): 1516–1523. Web.
- [22] Jones, B.F. "A Reappraisal of the Use of Infrared Thermal Image Analysis in Medicine." *IEEE transactions on medical imaging* 17.6 (1998): 1019–1027. Web.

- [23] King, Davis E. "Dlib-ml: A machine learning toolkit." *The Journal of Machine Learning Research* 10 (2009): 1755-1758. Web.
- [24] Kiritat, Ayca et al. "FLIR Vs SEEK Thermal Cameras in Biomedicine: Comparative Diagnosis through Infrared Thermography." *BMC Bioinformatics* 21.Suppl 2 (2020): 88–88. Web.
- [25] Kong, Seong G. et al. "Recent Advances in Visual and Infrared Face Recognition—a Review." *Computer vision and image understanding* 97.1 (2005): 103–135. Web.
- [26] Kontos, M, R Wilson, and I Fentiman. "Digital Infrared Thermal Imaging (DITI) of Breast Lesions: Sensitivity and Specificity of Detection of Primary Breast Cancers." *Clinical radiology* 66.6 (2011): 536–539. Web.
- [27] Kuzdeuov, Askat et al. "SF-TL54: A Thermal Facial Landmark Dataset with Visual Pairs." 2022 IEEE/SICE International Symposium on System Integration (SII). IEEE, 2022. 748–753. Web.
- [28] Lahiri, B.B. et al. "Medical Applications of Infrared Thermography: A Review." *Infrared Physics & Technology* 55.4 (2012): 221–235. Web.
- [29] Martinez-Jimenez, Mario A. et al. "Diagnostic Accuracy of Infrared Thermal Imaging for Detecting COVID-19 Infection in Minimally Symptomatic Patients." *European journal of clinical investigation* 51.3 (2021): e13474–n/a. Print.
- [30] Neamen, Donald A. *Semiconductor Physics and Devices: Basic Principles*. Fourth edition. New York, NY. McGraw-Hill, 2012. Print.
- [31] Negishi, Toshiaki et al. "Contactless Vital Signs Measurement System Using RGB-Thermal Image Sensors and Its Clinical Screening Test on Patients with Seasonal Influenza." *Sensors* 20.8 (2020): 2171–. Web.
- [32] Nginx for Windows. *Nginx*, <https://nginx.org/en/docs/windows.html>. Feb 17, 2023. Web.
- [33] Poh, Ming-Zher, Daniel J McDuff, and Rosalind W Picard. "Advancements in Noncontact, Multiparameter Physiological Measurements Using a Webcam." *IEEE transactions on biomedical engineering* 58.1 (2011): 7–11. Web.
- [34] Qiu, P. F., S. Y. Zhang, and X. J. Shui. "Photoacoustic Study of Thermal Properties of Biological Tissues Detected by PVDF Film Transducer." *The European physical journal. ST, Special topics* 153.1 (2008): 487–490. Web.
- [35] Ring, E. F. J., and K Ammer. "Infrared Thermal Imaging in Medicine." *Physiological measurement* 33.3 (2012): R33–R46. Web.

- [36] Ring, E. F. J. et al. “NEW STANDARDS FOR FEVER SCREENING WITH THERMAL IMAGING SYSTEMS.” *Journal of mechanics in medicine and biology* 13.2 (2013): 1350045–1350012. Web.
- [37] Ring, E.F.J. “The Historical Development of Temperature Measurement in Medicine.” *Infrared physics & technology* 49.3 (2007): 297–301. Web.
- [38] Ring, Francis J. “Pioneering Progress in Infrared Imaging in Medicine.” *Quantitative infrared thermography* 11.1 (2014): 57–65. Web.
- [39] Sarigoz, Talha et al. “Role of Digital Infrared Thermal Imaging in the Diagnosis of Breast Mass: A Pilot Study; Diagnosis of Breast Mass by Thermography.” *Infrared physics & technology* 91 (2018): 214–. Web.
- [40] Strang, Gilbert. *Introduction to Linear Algebra*. 5th ed. Wellesley - Cambridge Press, 2016. Print.
- [41] Syed Muslim, Jameel et al. “Automatic Image Annotation for Small and Ad Hoc Intelligent Applications Using Raspberry Pi.” *MATEC Web of Conferences* 255 (2019): 1003–. Web.
- [42] Tan, Jen-Hong et al. “Infrared Thermography on Ocular Surface Temperature: A Review.” *Infrared physics & technology* 52.4 (2009): 97–108. Web.
- [43] Topdon Thermal Infrared Camera TC001. *Topdon Technology Co., Ltd*, <https://www.topdon.com/products/tc001>. Feb 17, 2023. Web.
- [44] Vainer, Boris G. “A Novel High-Resolution Method for the Respiration Rate and Breathing Waveforms Remote Monitoring.” *Annals of biomedical engineering* 46.7 (2018): 960–971. Web.
- [45] Zhang, Zuopeng et al. “Infrared Thermal Imaging of Patients with Acute Upper Respiratory Tract Infection: Mixed Methods Analysis.” *Interactive journal of medical research* 10.3 (2021): e22524–e22524. Web.
- [46] Zoukhri, Driss. “Effect of Inflammation on Lacrimal Gland Function.” *Experimental eye research* 82.5 (2006): 885–898. Web.

Appendix A: Block Diagram of Processing a Video Stream

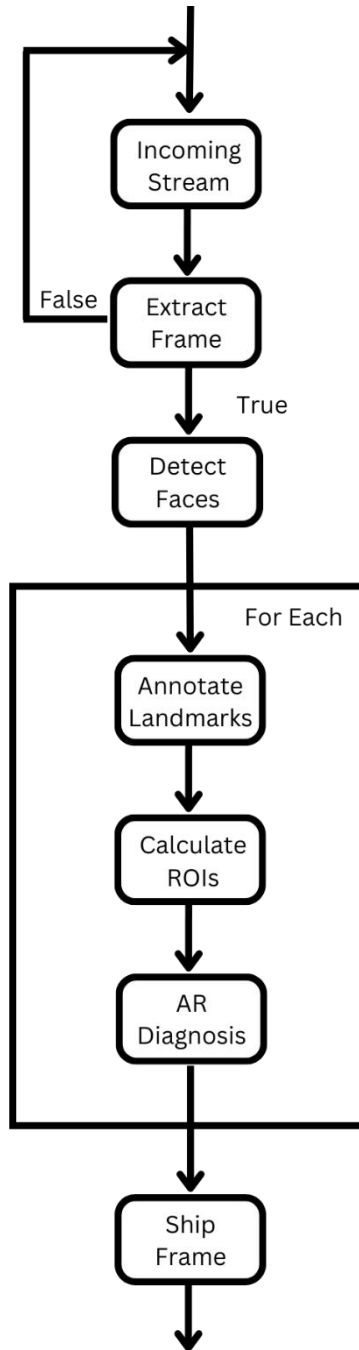


Figure A.1: Block diagram illustrates the processing of a video stream. Note it happens frame by frame.

Appendix B: Doll Head Simulation



Figure B.1: Doll head simulation with negative AR diagnosis.



Figure B.2: IR doll head simulation showing negative ROIs.



Figure B.3: Doll head simulation with positive AR diagnosis.



Figure B.4: IR doll head simulation showing positive ROIs.

Appendix C: Nasolacrimal Vector

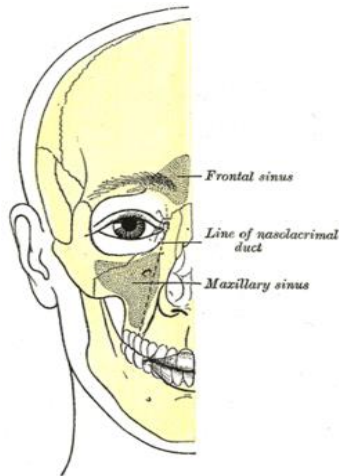


Figure C.1: Side profile of human face. Illustrates the sinus location and the vector of the nasolacrimal duct. Reprinted from [12]. Public Domain.

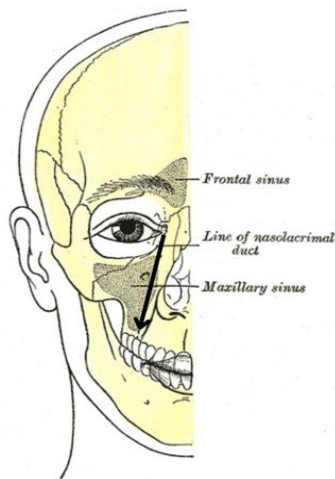


Figure C.2: The nasolacrimal vector drawn on side profile of human face. This vector is used to draw the nasolacrimal ducts on subsequent images to compare with facial landmark locations. Modified from [12]. Public Domain.

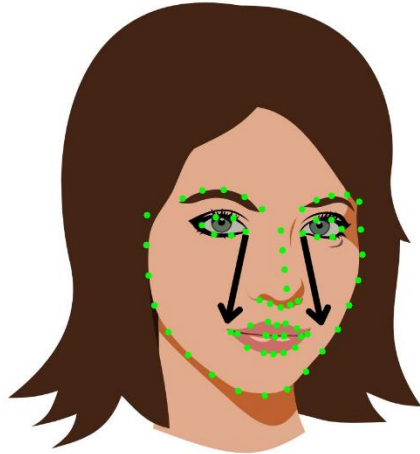


Figure C.3: The nasolacrimal vector drawn on an RGB diagram. Facial landmarks illustrate vector positioning.

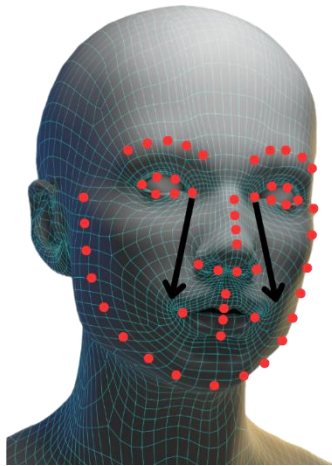


Figure C.4: The nasolacrimal vector drawn on an IRT diagram. Example model to illustrate anatomical locations more clearly.



Figure C.5: TOPDON TCView TC001 thermal image with facial landmarks.



Figure C.6: TOPDON TCView TC001 thermal image with nasolacrimal vector.

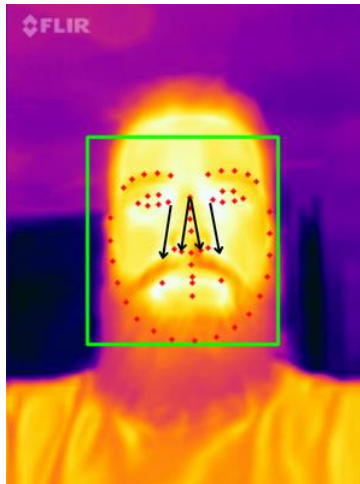


Figure C.7: Positive FLIR ONE Pro thermal image with nasolacrimal vector.



Figure C.8: Positive FLIR ONE Pro thermal image with nasolacrimal ROI. Region is selected to avoid high temperatures surrounding the lacrimal caruncles.

Appendix D: Kiosk and Mobile Diagrams

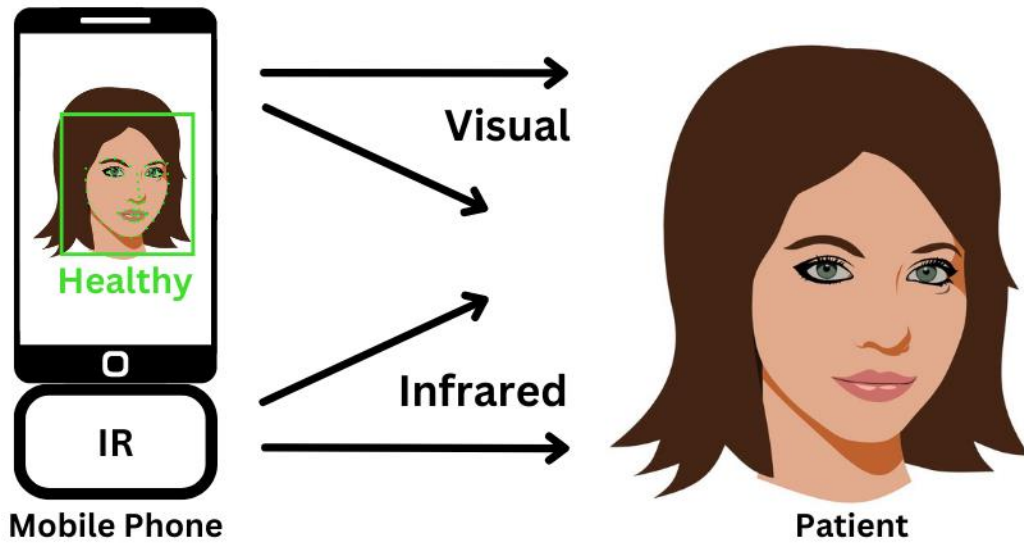


Figure D.1: Diagram illustrating the mobile app for augmented reality diagnosis. The different camera resolutions of various mobile devices will depend on a reliable homography matrix.

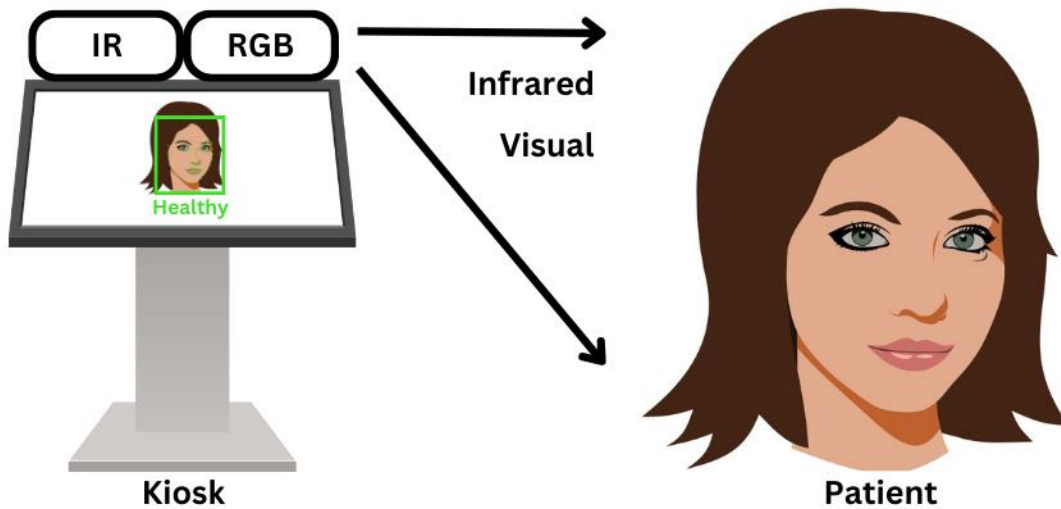


Figure D.2: Diagram illustrating the kiosk device for augmented reality diagnosis. Uniform distances between the cameras and pixel resolution will improve the homography matrix results.

Appendix E: Kiosk and Mobile Prototypes



Figure E.1: Android mobile phone prototype demonstration.



Figure E.2: Kiosk prototype demonstration.